An embryonic fold and thrust belt south of the Himalayan morphological front: examples from the Central Nepal and Darjeeling piedmonts

Jean-louis Mugnier, P Huyghe, E Large, F Jouanne, B Guillier, T Chakraborty

An embryonic fold and thrust belt south of the Himalayan morphological front:

examples from the Central Nepal and Darjeeling piedmonts

J-L. Mugnier [a]*, P. Huyghe [a], E. Large [a], F. Jouanne a, B. Guillier [a] and T. Chakraborty [b]

[a]*Institut des Sciences de la Terre, Université Grenoble Alpes/ Université Savoie Mont-Blanc/CNRS/IRD, CS40700, 38058 Grenoble Cedex 9, France;* [b]*Geological Studies Unit, Indian Statistical Institute, Kolkata 700108, India*

***Corresponding author: J.-L. Mugnier; jemug@univ-smb.fr**

Institut des Sciences de la Terre, Université Savoie Mont-Blanc/CNRS, 73376 Le Bourget-du-Lac Cedex, France

Abstract:

The morphological boundary between the Himalayas and the foreland plain is well expressed and most often corresponds to the frontal emergence of the Main Himalayan Thrust (MHT). This boundary is affected by surface ruptures during very large Himalayan earthquakes (Mw > 8) that regularly induce (with a recurrence of the order of 500 to 1,200 years) the uplift of the foothills relative to the plain.

However, a thrust-fold system is hidden beneath the plain and is displayed by the seismic profiles of oil companies in east/central Nepal and by H/V passive geophysical techniques in Darjeeling. Its long-term kinematic evolution is slow, with a tectonic uplift of the hanging wall that is lower than the subsidence rate of the foreland basin, that is, less than approximately half a millimetre per year. During phases of low sedimentation controlled by climatic fluctuations, the morphological surfaces of the piedmont are incised by large rivers for several tens of metres; therefore, structures hidden under the sediments emerge slightly in the plain.

The evolution of the hidden structures corresponds to an embryonic thrust belt mainly affected by a long-term shortening rate of $1.4\ ^{+2.5}/_{-1.2}$ mm·yr^{-1}, that is, 2–20% of the shortening rate of the entire Himalayan thrust system. Nonetheless, the details of the deformation associated with the embryonic thrust belt are still poorly understood. Several deformation components could affect the central Himalayan and Darjeeling piedmonts. i) Any slow steady-state deformation, such as layer parallel

shortening (LPS) is not detected by Global Navigation Satellite System (GNSS) data, and such deformation would therefore absorb less than 0.5 mm·yr^{-1}. The geodetic data that suggest the aseismic growth of some of the structures are highly controversial. ii) For the rest of the deformation of the embryonic thrust wedge, it is yet to be proven whether deformation occurs during rare great earthquakes affecting the piedmont during medium earthquakes and/or during post-seismic deformation related to great earthquakes. The amplitude of this long-term low deformation is too limited to significantly reduce the seismic hazard in the seismic gaps of the Himalayan belt. iii) In some portions of the Himalayan front, such as Darjeeling (India), the thrust deformation related to great earthquakes propagates several tens of kilometres south of the morphological front in the zone previously affected by the long-term low deformation. It induces multi-metre surface ruptures in the piedmont and a mean shortening of 8.5 ± 6.2 mm·yr^{-1}. iiii) Pre-existing faults in the bedrock of the Indian craton, often oblique to the Himalayan structures, are locally reactivated beneath the foreland plain with low deformation rates.

Keywords: Himalayan mountain front, piedmont, foreland, blind thrusts, geomorphology, embryonic thrust wedge, layer parallel shortening

1. Introduction

The present-day tectonics of the Himalayas are characterised by the under-thrusting of the Indian lithosphere along the Main Himalayan Thrust (MHT) (Zhao et al., 1993) (Fig. 1). Himalayan tectonics are believed to follow a simple seismic cycle that displays a succession of ruptures along the MHT and finally transfers the entire convergence to the front of the Himalayas during giant earthquakes (e.g., Bilham, 2019; Dal Zilio et al., 2019). Therefore, the Holocene shortening of the Himalayas is frequently considered as almost entirely concentrated in the frontal thrust ramp, namely, the main frontal thrust (MFT) (e.g., Lavé and Avouac, 2000).

This is contrary to the shortening of numerous accretionary wedges and active mountain belts that are not currently concentrated in a unique frontal zone, but are distributed in an embryonic thrust zone (e.g., Le Béon et al., 2019; Gonzalez-Mieres and Suppe, 2011).

The incipient structures observed ahead of numerous active thrust belts or accretionary prisms are characteristic of embryonic thrust belts (Gonzalez-Mieres and Suppe, 2011). They are related to slow tectonic processes (Gonzalez-Mieres and Suppe, 2011) and frequently match large-scale pure shear deformation, classically defined as regional layer parallel shortening (LPS) (e.g., Mitra, 1994). Furthermore, detachment folds grow and induce heterogeneous layer-parallel thickening (Mitra, 2003). As shortening accumulates, the fold limbs steepen (Suppe et al., 2004) and the folds may evolve into classical fault-bend folds with ramps that accommodate kilometres of slip (Suppe, 1983). An aseismic deformation component has been suggested in the embryonic thrust belt ahead of the Taiwan thrust belt (Le Béon et al., 2019), but the link between the fold development and seismic cycle is still poorly understood (Suppe, 2014). Nonetheless, numerical modelling suggests that folding does not occur steadily over time, but is modulated by earthquake cycle stresses (Mallick et al., 2021).

Nonetheless, various surface deformations have been observed both at the sharp morphologic mountain front and south in the piedmont that forms the northern part of the Ganga and Brahmaputra plains. In numerous cases (Fig. 1A), weak tectonic uplift has been observed in the piedmont (e.g., Thakur et al., 2020; Srivastava et al., 2017; Kar et al., 2014; Yeats and Thakur, 2008) south of portions of the morphologic front where the palaeo-seismological activity of the Main Frontal Thrust (MFT) has been documented (e.g., Le Roux-Mallouf et al., 2020; Wesnousky et al., 2019; Kumar et al., 2006). This uplift of the piedmont is, in some cases, linked to the lateral propagation of the frontal thrust (e.g., Almeida et al., 2018; Delcaillau et al., 2006; Champel et al., 2002), but in most cases, it is located ahead of the frontal thrust (e.g., Thakur et al., 2020; Yeats and Thakur, 2008). Present-day deformation in the proximal foreland has been suggested by spirit levelling data (Jackson and Bilham, 1994), radar interferometry

(Bhattacharya et al., 2014; Yhokha et al., 2015), and GNSS data (Mullick et al., 2009); Gupta et al., 2017), but none of these studies are robust (Bilham et al., 2017). Further south, alluvial surfaces are uplifted, warped, and tilted and may form scarps up to 20 m (e.g., Pati et al., 2012). Some of the scarps were investigated using ground-penetrating radar and were attributed to the surface extent of thrust splays parallel to the Himalayan front (Yeats and Thakur, 2008) or oblique faults (Pati et al., 2012), with the latter likely linked to the reactivation of deeply buried ridges (e.g., Godin and Harris, 2014). Petroleum seismic reflection profiles (Duvall et al., 2020; Yeats and Thakur, 2008; Bashyal, 1998; Raiverman et al., 1994) and passive seismic data (Large et al., accepted) suggest that the top of the Middle Siwalik is folded and/or faulted by an incipient deformation linked to an embryonic thrust wedge south of the MFT.

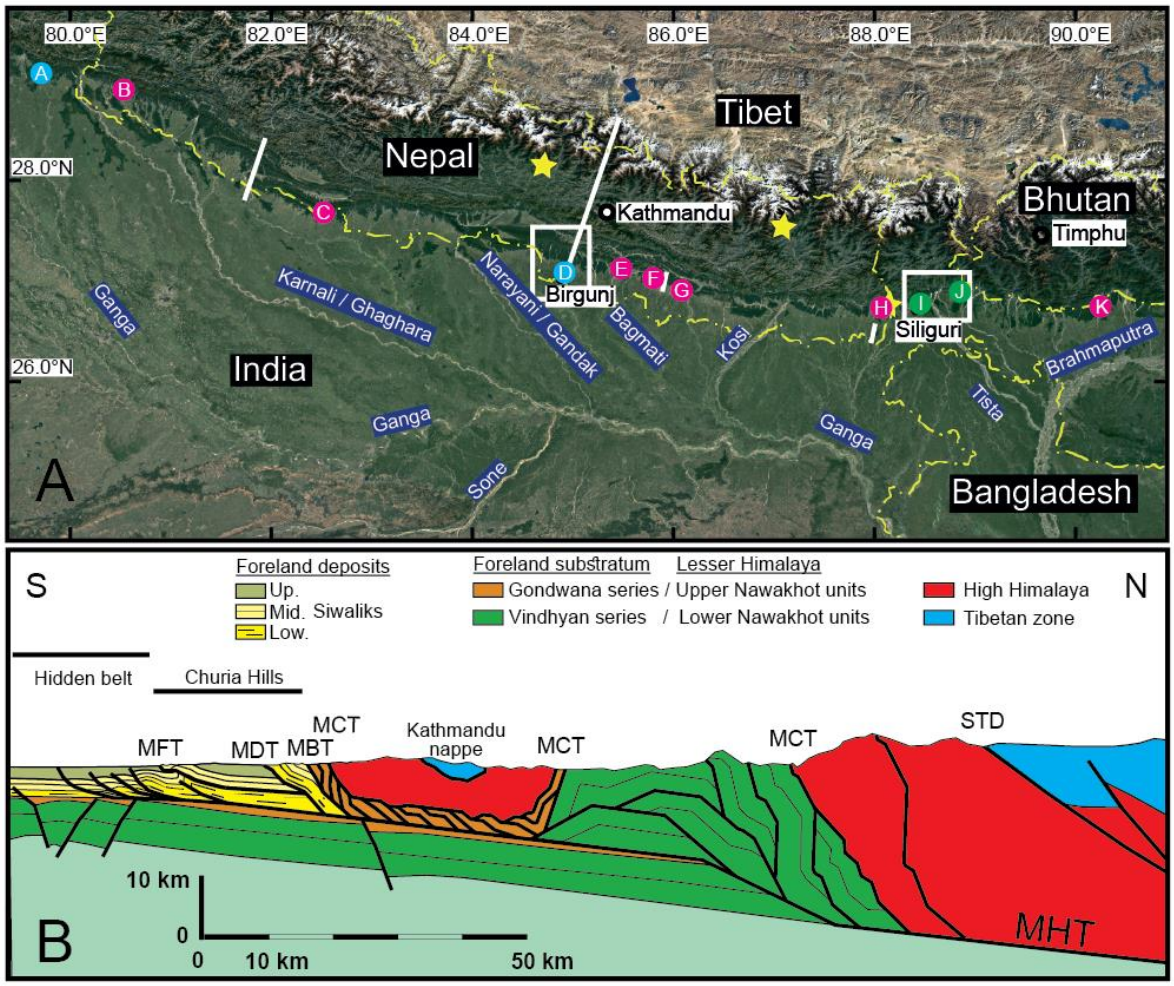

Figure 1: Overview map and cross-section of the areas of interest. (A) Satellite image of the Himalayan orogeny. The white boxes show the two study areas. The white lines indicate, from west to east, the location of the cross-sections of Fig. 2A, Fig. 1B, and Figs 3B and 3A. Circles A to J represent the combination of recent deformation south of the MFT and of the recent activity of the MFT from previous studies (see Table 2 for their description). The red circles represent geologic evidence of both the slightly uplifted zone in the piedmont and seismic rupture on the MFT. The green circles represent evidence of seismic rupture in the piedmont, and the yellow stars show the instrumental epicentres of Mw >8 earthquakes [1934 AD and 2015 AD earthquakes, from Bilham (2019)]. (B) Structural cross-section of the Himalayas [modified from Mugnier et al. (2017), Pearson and DeCelles (2005), and Bashyal (1998)]. MFT: Main Frontal Thrust; MDT: Main Dun Thrust; MBT: Main Boundary Thrust; MCT: Main Central Thrust; STD: South Tibetan Detachment; MHT: Main Himalayan Thrust.

Many studies have been conducted in the Himalayan piedmont (Table 2), but only a few have systematically compared imaged structures beneath the plain with the current surface deformation documented by geomorphological studies. In this study, we associated the surface deformations of the Himalayan proximal foreland south of the mountain front to the deep structures in two key zones (Fig. 1A). One is in east-central Nepal (Birgunj area), close to one of the best-studied cross-sections throughout the Himalayas (Fig. 1B) (e.g., Mugnier et al., 2017; Pearson and DeCelles, 2005; Lavé and Avouac, 2000) and the other is in Darjeeling/India (Siliguri area), where one of the best pieces of evidence of piedmont deformation through propagating thrust faults has been studied for a long time (Nakata, 1989). In addition to previous works concerning deformed surfaces and drainage system anomalies, we developed an analysis of river incision using a digital elevation model to quantify surface deformation. For the deep structures, we referred to a recent ambient seismic noise study as well as numerous published seismic reflection studies. The comparison between the geometry of the subsurface structures and the geomorphology shows that uplifted alluvial surfaces are located above an embryonic thrust and fold belt in the Birgunj and Siliguri areas. A quantitative analysis of the tectonics of the embryonic thrust wedge was performed by first estimating the uplift and then by estimating the shortening using simple kinematic models and balancing procedures. Indeed, although shortening is subject to more uncertainty than uplift, it allows for an easier comparison with the

general evolution of the Himalayan belt. Fold and thrust belt structures have been analysed for over 50 years (e.g., Butler, 2020, 1982; Boyer, S. E., and Elliott, D. 1982, Dahlstrom, 1970), and the kinematic models used in this paper have been developed and tested in regions where foreland basin sediments have been incorporated into fold and thrust belts (e.g., Le Béon et al, 2019; Suppe, 2014, 1983; Gonzalez-Mieres and Suppe, 2011, 2006; Suppe et al, 2004; Husson and Mugnier, 2003; Lavé and Avouac, 2000; Suppe and Medwedeff, 1990). These previous works limit interpretations of structural geometry to a narrow range of possible shapes in the areas studied in this paper where geometric observations are rare. Nevertheless, we have favoured the classical method of excess areas (Goguel, 1952; Chamberlin, 1910), which remains powerful (Moretti and Callot, 2012) even in such a case. In addition, special attention was paid to the uncertainties associated with the shortening estimate. Our results show that the embryonic thrust belt in the east/central Himalayas deformed at a slow rate, whereas the hidden belt in Darjeeling has recently deformed faster and is affected by large earthquake ruptures.

Our study improves and contributes to the knowledge on deformation in the Himalayan range. A better understanding of the seismic cycle, development of the embryonic thrust belt, and their relationship in a continental subduction range is of academic interest. Furthermore, the aseismic deformation near and south of the MFT is inconsistent with three decades of GPS data and most of the theoretical models of the genesis of great Himalayan earthquakes (Bilham et al., 2017; Dal Zillo et al., 2019), although some physical models (Berger et al., 2004) involving aseismic slip on the entire décollement were consistent with the previous and controversial levelling data (Jackson and Bilham, 1994). Therefore, identifying the seismogenic active structures and understanding the propagation in the foreland of seismic ruptures at a greater time scale than the seismic cycle is of utmost importance for assessing seismic hazards in this region, where the seismic risk is of significant societal importance owing to the high population density in these areas.

148 *Table 1 List of abbreviations in the text*

FAULTS	
MHT	Main Himalayan Thrust
MFT	Main Frontal Thrust
MFT1 to MFT6	Different fault segments of the MFT
MDT	Main Dun Thrust
MBT	Main Boundary Thrust
RT	Ramgarh Thrust
GTF	Gish Transverse Fault
R1	Basement fault inferred from the Birgunj geophysics
F2	Main thrust inferred from the Birgunj geophysics
Tf	Tista thrust inferred from the Tista River geophysics
TERRACES	
T1 to T4	River terraces in the Darjeeling area
TECHNICS AND CONCEPTS	
LPS	Layer Parallel Shortening
GNSS	Global Navigation Satellite Systems
Mw	Moment magnitude of an earthquake
GEOMETRIC PARAMETERS	
S	Shortening at the trailing edge
S_f	Sliding along a ramp
ΔA	Excess area
ΔAr	Increment of relief growing
T_0	Initial Thickness
T_{0r}	Thickness at the trailing edge
U	Uplift
θ	Dip of the ramp
V_{sed}	Long-term sedimentation rate at the footwall
V_{upl}	Uplift rate at the hanging wall

149

150 ## 2. Geological setting of the Himalayas

151

152 ### 2.1. The structure of the Himalayan range

153 The Himalayas are formed by a stack of thrust sheets (Le Fort, 1975) separated by major
154 north-dipping faults that branch off the main Himalayan thrust (MHT) (Fig. 1B). In the southern
155 part, the Lesser Himalayan domain overthrusts the sedimentary rocks of the Neogene Foreland
156 Basin (Siwaliks) along the Main Boundary Thrust (MBT) system and displays complex
157 duplexes in both the lower and upper Nawakhot units (DeCelles et al., 1998; Stöcklin, 1980).
158 The Siwaliks overthrust the modern foreland basin (Indo-Gangetic and Brahmaputra alluvial
159 plains) along the Main Frontal Thrust (MFT). Several thrusts have developed in the Siwaliks,
160 the major one being the Main Dun Thrust (MDT). Although out-of-sequence episodes have

occurred (Wobus et al., 2005; Hodges et al., 2004; Mugnier et al., 2004), the entire Himalayan fault system essentially propagates towards the south (e.g., DeCelles et al., 1998). The MHT absorbs approximately 18–20 $mm \cdot yr^{-1}$ of convergence in Nepal (Mugnier and Huyghe, 2006; Lavé and Avouac, 2000; Bilham et al., 1997), and more in eastern Assam (Burgess et al., 2012). The geometry of the MHT is characterised by a southern frontal ramp (the MFT) (e.g., Schelling and Arita, 1991), a shallow décollement at the boundary between the Indian Craton and the syn-orogenic sediments of the Siwaliks (Mugnier et al., 1999a), a detachment beneath the Lesser Himalayas, a crustal ramp cutting through the crust of the Indian craton (Avouac et al., 2001), and a lower flat that extends far to the north beneath the Tibetan Plateau (Fig. 1B).

2.2. The frontal structure of the Himalayan range

The forward propagation of the Himalayan deformation resulted in the inversion of the Neogene Siwalik Foreland Basin and a thin-skinned thrust belt forming the Churia Hills. The large-scale structures (Fig. 2A) consist of a series of asymmetric fault-related folds with a steep frontal limb, which is frequently completely eroded, and a preserved northern limb that dips 20–30° northward (Mugnier et al., 1999a).

In the field, the hanging wall of the MFT is parallel to the bedding at the base of the Lower Siwalik series, and restoration procedures suggest that the footwall flat lies at a depth of approximately 5 km below the Churia Hills in the central Himalayas (Lavé and Avouac, 2000; Mugnier et al., 1998). This result agrees with the interpretation of seismic lines in the western Himalayas (Powers et al., 1998). A shallower décollement has also been documented at a depth of approximately 2 km in the Middle Siwaliks in Nepal (Fig. 3) (Almeida et al., 2018; Schelling and Arita, 1991), and the superposition of décollements leads to a complex duplex-like geometry (Powers et al., 1998).

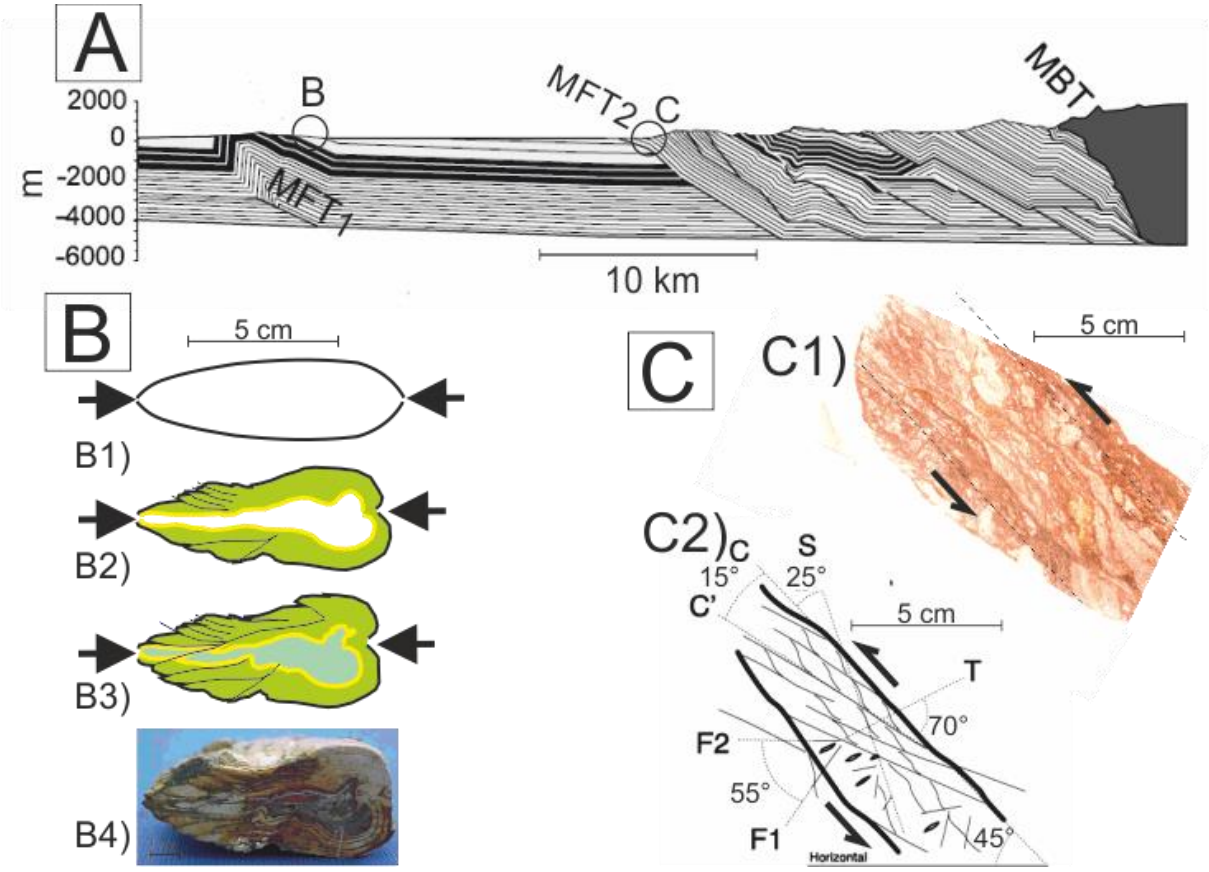

Figure 2: Types of deformation at the front of the Himalayas from examples of western Nepal. (A) Cross-section through the Siwalik beds of the Churia range [adapted from Mugnier et al. (1999a)] illustrating the succession of fault-propagation folds and folds where only the syncline part is preserved. The circles B and C refer to the location of samples B and C. (B) Internal layer-parallel shortening recorded by the deformation of a bivalve fossil. B1, B2, and B3: progressive deformation from the initial bivalve till the final geometry. The green and yellow levels refer to progressive calcite filling of the shell and (B4) section through the fossil. (C) Simple shear deformation related to major thrusts with C1) showing the section through a shear zone and C2) showing an interpretation of the deformation features in the shear zone. S: pressure solution cleavage; C and C' Riedel fractures; T Tension crack; F1 and F2 late small-scale fractures [from Mugnier et al. (1998)].

The MFT is considered to be the youngest and southernmost thrust of the Himalayan fault system, although other structures have been imaged beneath the plain using seismic reflection profiles (e.g., Duvall et al., 2020). In particular, incipient triangular zones related to back-thrust (Fig. 3A) (von Hagke and Malz, 2018) and folds related to the initial stage of fault propagation (Suppe and Medwedeff, 1990) are locally found on the frontal structures (Fig. 3B)

(Almaida et al., 2018). Furthermore, the MFT reaches the surface in most cases at the sharp topographic front of the range, but has also been observed at the base of smaller reliefs in the piedmont of eastern Nepal (Delcaillau, 1986), Darjeeling (India) (Nakata, 1989), and Bhutan (Dasgupta et al., 2013). Specifically, the MFT is not a continuous fault throughout the entire range, but consists of a succession of segments that branch on each other or depict an echelon pattern (Mugnier et al., 1999a; Delcaillau, 1986). This segmentation is partly controlled by subsurface basement structures beneath the foreland sediment (Divyadarshini and Tandon, 2022). A numbering system is frequently used to define different fault segments, such as MFT1 to MFT3 in western Nepal (Mugnier et al., 1999a), MFT1 to MFT6 in central Nepal (Divyadarshini and Singh, 2019), and MFT1 to MFT4 in the Darjeeling area (Large et al., accepted).

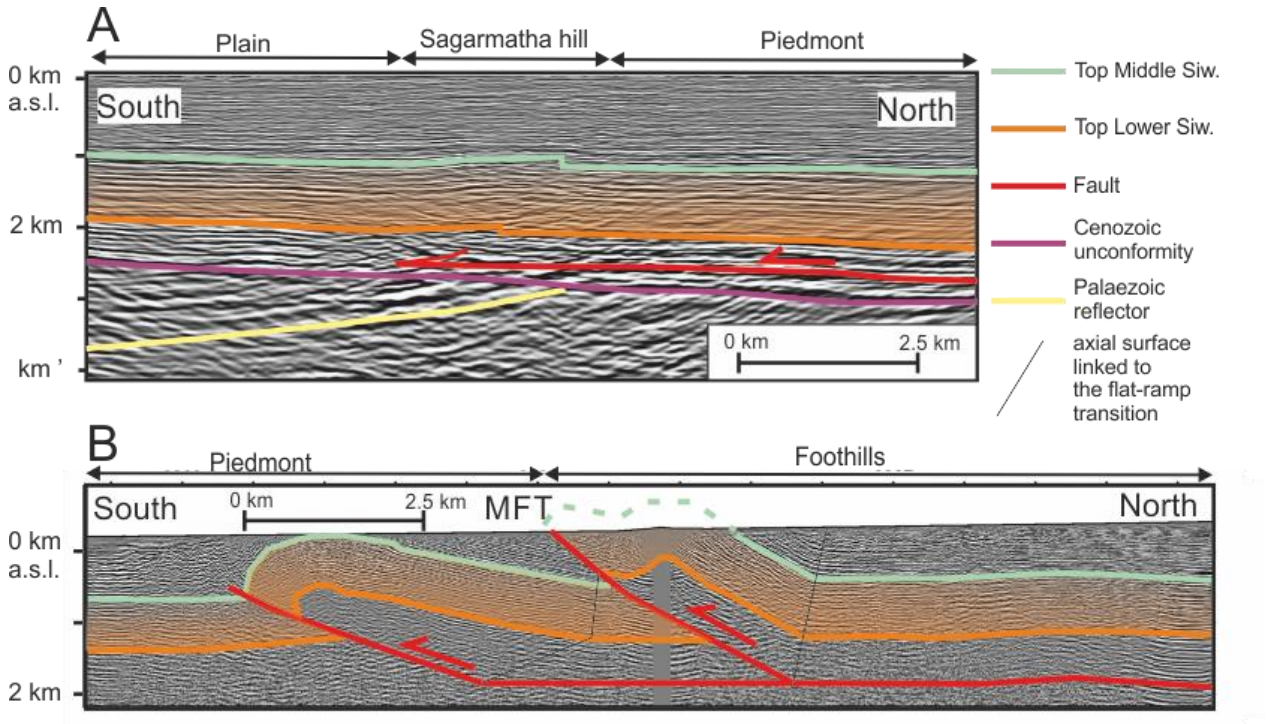

Fig. 3. Structures imaged by seismic lines (location on Fig. 1A), A) in the piedmont [adapted from Duvall et al. (2020)] and B) at the front of Himalayas [adapted from Almaida et al. (2018)].

Thrust faults are formed by very narrow (a few tens of centimetres to a few metres) shear zones (Fig. 2C), and the superimposition of a cataclastic deformation in the vicinity of the faults (Mugnier et al., 1998) on a pressure-solution deformation suggests discontinuous slip during earthquakes (Gratier and Gueydan, 2007). The deformation in the thrust sheets is mainly related to their motion above the fault system, but layer parallel shortening (LPS) is evidenced by the preferred orientation of the grain shape (Srivastava and Mukul, 2020) and the deformation of rare fossils (Fig. 2B). Furthermore, the geometries of the folds linked to fault propagation (Fig. 3B) suggest that axial surfaces above the flat-ramp transition are sheared, and that internal deformation occurs within the levels located above the décollement (Suppe et al., 2004).

2.2.1. Late Pliocene to Pleistocene formation of the MFT

In the western Himalayas (Pakistan), frontal structures developed as early as 2.5 Ma (Pennock et al., 1989) and are absorbing the Himalayan shortening at a rate of 8.4 ± 1 mm·yr^{-1} (Cortés-Aranda et al., 2017; McDougall et al., 1993). In western and central Nepal, the MFT has been developing since 2 Ma, as evidenced by syn-tectonic sedimentation (Mugnier et al., 2004) and apatite fission track analysis (Robert, 2009; Van der Beek et al., 2006). A Holocene slip rate of 19 ± 6 mm·yr^{-1} to 21 ± 1.5 mm·yr^{-1} was established for the frontal zone of the Siwaliks (Mugnier et al., 2004; Lavé and Avouac, 2000). In the eastern Himalayas, the MFT was initiated later than 1 Ma (Chirouze et al., 2013) and a minimum slip of 23.4 ± 6.2 mm·yr^{-1} was established for the MFT throughout the Holocene (Burgess et al., 2012). The Quaternary propagation of the front induces piggyback basins (Ori and Friend, 1994), locally known as duns, in numerous portions of the Himalayas.

246 2.2.2. The Himalayan seismic cycle and the recent activity of the Main Frontal
247 Thrust

248 The only surface rupture observed in the field for a Himalayan earthquake was linked
249 to the 7.6 Mw 2005 Kashmir earthquake, but was along the MBT (Kaneda et al., 2008). Even
250 for the 8.4 Mw 1934 Eastern Nepal earthquake or the 8.4 Mw 1950 Assam earthquake, no direct
251 observations of their surface ruptures were archived, and they were only inferred from trenching
252 studies performed by Sapkota et al. (2013) and Priyanka et al. (2017).

253 Nonetheless, historical archives of the damage (e.g., Bilham, 2019) and palaeo-
254 seismological trenches (e.g., Kumar et al., 2010) indicate that large earthquakes with >8
255 moment magnitude (M) have episodically ruptured several hundred-kilometre-long segments
256 of the southern part of the MHT (Chandra, 1992). The magnitude of the highest events remains
257 a matter of debate (e.g., Mugnier et al., 2013), particularly in the seismic gaps underlined by
258 historical seismicity (e.g., Bilham, 2019; Seeber and Armbruster, 1981). The areas within the
259 scope of this study are located in major seismic gaps in central Nepal and Darjeeling (Bilham,
260 2019).

261 Most of our knowledge about earthquakes that ruptured the MFT is summarised in a
262 conceptual model based on palaeo-seismology, tectonic geomorphology, historical archives,
263 and geodesy (Bilham, 2019). In this model, large earthquakes (typically Mw ~ 8) rupture the
264 entire length of the MHT from its downdip to the external part (Dal Zilio et al., 2019). They
265 uplift (Avouac et al., 2001) and deform (Whipple et al., 2016) the entire Himalayas. Most of
266 them reach the emerging MFT and delineate the morphologic front; however, it remains
267 uncertain whether all great earthquakes reach the surface (Wesnousky et al., 2018).

268 The along-strike distribution of large earthquakes remains largely debated (e.g., Pierce
269 and Wesnousky, 2016; Mugnier et al., 2013). In the studied zone, between the 1505 AD west
270 Nepal earthquake rupture zone (Yule et al., 2006) and eastern Bhutan, no historic earthquake
271 clearly ruptured the MFT. The respective extensions of 1255 AD (Mishra et al., 2016; Sapkota

et al., 2013) or approximately 1100 AD (Kumar et al., 2010; Lavé et al., 2005) ruptures remain under discussion. Similarly, the 1934 AD Bihar Nepal earthquake surface rupture was initially inferred to extend more than 100 km along the MFT (Sapkota et al.; 2013), an interpretation later disproved by Wesnousky et al. (2018). Therefore, the initial hypothesis of a rupture of the 1934 earthquake extending under the plain (e.g., Seeber and Armbruster, 1981; Dunn et al., 1939) cannot be definitively discarded because it remains in agreement with geodetic data and with the strong aftershock located near the Indian border, four days after the main earthquake (Bilham et al., 1998).

Several observations suggest the occurrence of giant earthquakes greater than ~8.4 Mw historical events, because the great earthquakes of the past three centuries are insufficient to explain the transfer of the measured convergence towards the frontal thrust belt (Bilham, 2001) and because seismological trenching is indicative of events with more than 10-m displacements (e.g., Sapkota et al., 2013; Kumar et al., 2010; Lavé et al., 2005) (Table 2). Giant earthquakes would rupture the entire locked part of the MHT, from its downdip up to the MFT surface outcrops, and transfer more than 10 m of displacement from the hinterland to the MFT with a recurrence of 500 to 1200 years (Bollinger et al., 2014).

Medium earthquake ruptures, typically Mw ≤ 7.8, only extend along a portion of the seismological MHT. They either reach the surface out-of-sequence, similar to the 2005 Kashmir earthquake (Kaneda et al., 2008), or end several tens of kilometres north of the MFT, similar to the 2015 Gorkha earthquake (Avouac et al., 2015). Their slip is larger than 4 m and locally reaches up to 9.6 m (Pathier et al., 2006) or 7 m (Grandin et al., 2015) (the Kashmir and Gorkha earthquakes, respectively). They transfer stress in the outer domains and lead to small thrust reactivations in the Churia range of a few tens of centimetres, which is two orders of magnitude below the total slip recorded along the MHT (Elliott et al., 2016). Stress loading of the MFT occurs on the lateral terminations of great earthquakes and south of medium earthquake ruptures. However, the release of stress loading remains poorly understood. This occurs when greater ruptures reach the MFT (Dal Zilio et al., 2019; Bilham et al., 2017), but numerous

observations (Table 2 and Appendix A: Supplementary data) suggest a complex deformation pattern beneath the piedmont.

2.3. The foreland of the Himalayan range

2.3.1. Geology of the Neogene to modern Himalayan foreland

Seismic data have imaged a thick Tertiary sedimentary wedge beneath the foreland plain in Nepal (e.g., Duvall et al., 2020; DMG, 1990) and India (e.g., Srinivasan and Khar, 1996; Raiverman et al., 1994), where wells have been drilled (e.g., Mugnier and Huyghe, 2006). The Tertiary sediments are thinned out southward and unconformably cover the Indian shield formed in the Late Palaeozoic to Mesozoic Gondwana series (lateral equivalent of the upper Nawakhot series of the Lesser Himalayas) or the Late Proterozoic to Early Palaeozoic Vindhyan series (lateral equivalent of the lower Nawakhot series).

The Tertiary sedimentary wedge consisted of two groups of foreland sediments. The oldest group is related to the thin Palaeocene to Miocene series, the oldest of which was deposited via a forebulge basin (DeCelles et al., 1998). The Siwalik group consists of mid-Miocene to Pleistocene molasses deposited in a foreland basin and nourished by the erosion of the hinterland mountains, which is traditionally divided into three lithologic units: the Lower, Middle, and Upper Siwaliks (Gansser, 1964). The total thickness of the three units is up to 5 km (Raiverman et al., 1994).

Table 2. Studies of active tectonics at the Himalayan morphological front and within the piedmont (from west to east).

	Site name	Latitude/ Longitude	Ref	Type of study	Description of the deformation	Type of structures	Label
1	Lilla	32.323556°N/72.274373°E	(1)	Seismic lines	Hidden fault-related anticline (Western syntax)	b1	
2	Pabbi Hills	32.770263°N/73.697979°E	(1)	Seismic lines	Emergent fault-related anticline (Western syntax)	b2	
3	Hajipur	31.978567°N/75.734766°E	(2)	Seismol. trenching	Seismic rupture along the MFT (lateral propagation)	a1	0
4	Bamonwal-Siprian	31.961803°N/ 75.710387°E	(2)	Geomorph. study	Degraded scarp ~3 km south of the MFT	b1?	
5	Bhatpur	31.304522°N/76.163889°E	(3)	Seismol. trenching	Seismic rupture along the MFT	a1	
6	Masol	30.916264°N/ 76.429419°E	(4b)	Geomorph. study	River diversion and degraded scarp x km south of the MFT	b1	0
7	Chandigarh	30.714666°N/76.873244°E	(4)	Seismol. trenching	Seismic rupture along the MFT	a1	
8	Kala Amb	30.473456°N/77.212165°E	(5)	Seismol. trenching	Seismic rupture along the MFT	a1	
9	Rampur Ganda	30.475024°N/77.213303°E	(4)	Seismol. trenching	Seismic rupture along the MFT	a1	
10	Saharanpur	30.034152°N/77.617100°E	(6)	Seismic lines	'Flower structures' above N-S basement faults	d	
11	Mohand	30.101817°N/77.884437°E	(7)	Radar interferom.	Present uplift expressed along the rivers	c2	0
12	Roorke	30.017155°N/77.873015°E	(1)	Geomorph. study	Tilted and uplifted piedmont –'Piedmont Fault'	b2, c1?	
13	Lal Dhang	29.848533°N/78.321797°E	(4)	Seismol. trenching	Seismic rupture along the MFT	a1	
14	Najibabad	29.677052°N/78.343195°E	(8)	Remote sensing	15-km uplifted zone-'subsurface Najibabad Fault'	b2, c1?	
15	Ramnagar	29.390559°N/79.127987°E	(4)	Seismol. trenching	Seismic rupture along the MFT	a1	
16	Haldwani	29.088890°N/79.690601°E	(9)	Radar interferom.	20-km present uplifted zone in the piedmont	c2	A
17	Tanakpur	28.846776°N/80.068869°E	(10)	Geomorph. study	Transverse active faults	d	
18	Mohana Khola	28.916808°N/80.527963°	(11)	Seismol. trenching	Seismic rupture along the MFT	a1	B
19	Sarda to Babai River	28.910824°N/80.131557°E 27.978155°N/81.694145°E	(12)	Remote sensing analysis	Western and eastern ends of a NW-SE lineament in the piedmont	b2?	
20	Babai River to to Tulsipur	27.779350°N/81.916719°E 27.539566°N/82.411773°E	(12)	Remote sensing analysis	Western and eastern ends of a WNW-ESE lineament in the piedmont	b2?	C
21	Koilabas	27.685344°N/82.526895°E	(13)	Geomorph. study	Seismic rupture along the MFT	a1	
22	Tribeni	27.454052°N/83.916384°E	(14)	Seismol. trenching	Seismic rupture along the MFT	a1	
23	Birg.-Hetauda road	27.081926°N/84.917899°E	(15)	Spirit levelling	30-km uplifted zones in the piedmont	c1	D
24	Birg.-Hetauda road	27.081926°N/84.917899°E	(16)	Seismic line	A hidden thrust splay	c2	
25	Birgunj	27.009030°N/84.870566°E	(17)	Seismic line	Basement fault reactivation	d	
26	Baghmati (front)	27.135514°N/85.487162°E	(14)	Seismol. trenching	Seismic rupture along the MFT	a1	E
27	Baghmati (plain)	26.323662°N/85.508750°E	(18)	Geomorph. study	Tectonic lineament in the piedmont	d	
28	Khayarmara	27.068840°N/85.797880°E	(19)	Seismol. trenching	Scarp 400 m south of the MFT	a2	
29	Marha Khola	27.051167°N/85.818206°E	(20)	Seismol. trenching	Scarp 1.2 km south of the MFT	a2	
30	Sir Khola	27.048373°N/85.871830°E	(21)	Seismol. trenching	Seismic rupture along the MFT	a1	F
31	Bhabsi River	27.019091°N/85.878766°E	(22)	Seismic lines	Fault-propagation anticline 3 km south of the mountain front	b2	
32	Gangetic plain	26.200081°N/85.921142°E	(23)	Geomorph. study	Topographic breaks in the plain	d	
33	Charnath-Aurahi	26.918399°N/86.082130°E	(24)	Seismol. trenching	MFT	a1	G
34	Ratmate	26.912765°N/86.090750°E	(24)	Geomorph. study	Blind thrust 500 m south of the mountain front	a2	
35	Damak	26.733000°N/87.699000°E	(25)	Seismol. trenching	MFT	a1	
36	Sagarmatha	26.467947°N/87.990733°E	(26)	Geomorph. study	Growing anticlinal 30 km south from the morphologic front	b1	H
37	Sagarmatha	26.467947°N/87.990733°E	(27)	Seismic line	Anticline above a back-thrust	b1	
38	Hokse	26.759746°N/88.074739°E	(28)	Seismol. trenching	MFT	a1	
39	Tokla Tea Estate	26.644997°N/88.185671°E	(28)	Geomorph. study	Anticlinal 15 km south from the morphologic front	b1	
40	Singhimuni	26.591722°N/88.204280°E	(28)	Seismol. trenching	Strike slip fault 20 km from the front	d	
41	Tista River	26.766499°N/88.519789°E	(29)	Geomorph. study	Two scarps 25 km south from the morphological front	a3	I
42	Siliguri area	27.081926°N/84.917899°E	(29)	Geophysical study	A hidden thrust splay	c2	
43	Samsing	26.990649°N/88.796921°E	(30)	Geomorph. study	Scarp (MBT) located above a fan	a1?	J
44	Matiali	26.941269°N/88.810272°E	(30)	Geomorph. study	Scarp (MFT1) located above a fan	b1	
45	Batabari	26.839273°N/88.819424°E	(31)	Geomorph. study	Lineament in the piedmont	b2?	
46	Chalsa area	26.872660°N/ 88.803580°E	(32)	GPS study	Geodesy through MFT1,MFT2, and MBT	a, b1	
47	Bharadighi	26.788411°N/88.839102°E	(30)	Geomorph. study	North facing scarp in the piedmont	d, b1?	
48	Panijhora	26.882931°N/88.853980°E	(33)	Seismol. trenching	Seismic ruptures (MFT2) located in the piedmont	a3	
49	Chalsa	26.880971°N/88.867943°E	(34)	Seismol. trenching	Seismic ruptures (MFT2) located in the piedmont	a3	
50	Piping	26.722853° N/89.759980°E	(35)	Seismol. trenching	Seismic rupture along the MFT	a1	
51	Lalbeti	26.744331°N/90.2°E	(36)	Geomorph. study	Fault-related anticline 15 km south of the front	b2	K
52	Sarpang	26.858934°N/90.257642°E	(37)	Seismol. trenching	Seismic rupture along the MBT	a1	
53	Kokrajhar area	26.562453°N/ 90.289895°E	(38)	GPS and geomorph.	Geodesy through MFT1 and a growing anticline	a1, b2	
54	Nameri	26.915017°N/92.752704°E	(34)	Seismol. trenching	Seismic rupture along the MFT	a1	
55	Harmutty	27.133190°N/93.850572°E	(34)	Seismol. trenching	Seismic rupture along the MFT	a1	
58	Himebasti	27.430368°N/94.201264°E	(39)	Seismol. trenching	Seismic rupture along the MFT	a1	
59	Marbong	27.973233°N/95.228520°E	(40)	Seismol. trenching	Seismic rupture along the MFT	a1	
60	Pasighat	28.078065°N/95.332326°E	(41)	Seismol. trenching	1950 AD seismic rupture along the MFT	a1	
61	Kamlang Nagar	27.757485°N/ 96.355718°E	(42)	Seismol. trenching	1950 AD seismic rupture (Mishmi Thrust, Eastern syntax)	a1	

The column-labelled site name is used for the location of the sites on Google Earth (see Appendix A: Supplementary data). The column-labelled Type of Structures refers to the diagrams proposed in Figure 15. a1) Geologic evidence of seismic rupture at the sharp transition between the Himalayas and the

piedmont; a2) seismic ruptures located less than 2 km from the sharp morphologic transition; a3) seismic ruptures in the piedmont (more than 2 km from the sharp morphologic transition); b1) hidden fault-related anticline that is submerged by the sediment and diverts river drainage; b2) emergent fault-related anticline incised by rivers; c1) hidden thrust splay; c2) monitoring of present-day uplifted zones in the piedmont; d) structures linked to basement fault reactivation. The column-labelled Label refers to the zones where several types of structures were found on the same transverse cross-section (location in Fig. 1A for the A to K labels, labelled 0 for the sites outside Fig. 1A). Reference column: (1) Yeats and Thakur (2008); (2) Malik et al. (2010); (3) Kumahara and Jayangondperumal (2013); (4b) Singh and Tandon, 2008; (4) Kumar et al. (2006); (5) Kumar et al. (2001); (6) Raiverman et al. (1994); (7) Bhattacharya et al. (2014); (8) Kralia and Thakur (2021); (9) Yhokha et al. (2015); (10) Goswami (2012); (11) Yule et al. (2006); (12) Misra et al. (2020); (13) Mugnier et al. (2005); (14) Wesnousky et al. (2017a); (15) Jackson and Bilham (1994); (16) Bashyal (1998); (17) DMG, 1990); (18) Jain et Sinha (2005); (19) Wesnousky et al. (2019); (20) Lavé et al. (2005); (21) Sapkota et al. (2013) and Wesnousky et al. (2018); (22) Almaida et al. (2018); (23) Pati et al. (2012); (24) Rizza et al. (2019); (25) Wesnousky et al. (2017b); (26) Sapkota (2011); (27) Duvall et al. (2020); (28) Upreti et al. (2000); (29) Large et al., in press; (30) Nakata (1989); (31) Srivastava et al. (2017); (32) Mullick et al. (2009); (33) Mishra et al. (2016); (34) Kumar et al. (2010); (35) LeRoux-Mallouf et al. (2020); (36) Dashgupta et al. (2013); (37) LeRoux-Mallouf et al. (2016); (38) Gupta et al. (2017); (39) Pandey et al. (2021); (40) Jayangondaperumal et al. (2011); (41) Priyanka et al. (2017); (42) Singh et al. (2021).

In some sections of Nepal (Mugnier et al., 1999a) and Darjeeling (Chakraborty et al., 2020), a clear angular unconformity is observed as the boundary between the Upper Siwaliks and an overlying Quaternary alluvium unit. Nonetheless, this boundary is often difficult to precisely define (Sinha et al., 2007; Jain and Sinha, 2003).

The sedimentary wedge beneath the foreland in the Nepal Himalayas is affected by numerous faults and fold structures related to an incipient fold and thrust system located above a décollement at the base of the Tertiary (Fig. 3B) (Duvall et al., 2020; Bashyal, 1998; Friedenreich et al., 1994). Furthermore, the Tertiary reactivation of basement faults has been locally imaged (Manglik et al., 2022; Adilakshmi et al., 2021). Similar tectonic features within the sedimentary wedge and its basement have also been found in western (e.g., Yeats and Takhur, 2008) and eastern India (Karunakaran and Rao, 1976).

359 2.3.2 Morphology of the Himalayan piedmont

360 The geomorphology and stratigraphic architecture of the Himalayan piedmont mainly
361 depend on mountain-fed, foothill-fed, and plain-fed river source areas (Sinha et al., 2010).
362 Megafans develop at the mountain exit of the major Himalayan rivers (Ghaghara, Gandak, Kosi,
363 and Tista Rivers on Fig. 1A) that transport prodigious quantities of detrital material. They are
364 spread over vast areas with low gradients and consist of multi-storied sand sheets (Chakraborty
365 and Gosh, 2010; Sinha et al., 2007).

366 Inter-megafan areas are drained by foothills and plain-feeding rivers. Furthermore, their
367 deposits correspond to overbank deposits forming mud-dominated intervals in the Quaternary
368 alluvium or small stream-dominated alluvial fans that extend south of the mountain front down
369 to 10–15 km, depositing locally coarse reworked material such as the Bagmati fan (Fig. 1A).
370 Therefore, deposits of the inter-megafan piedmont just south of the mountain exit consist of
371 poorly sorted boulders, cobbles, pebbles, and narrow sand bodies interbedded in muddy
372 sequences (Dhital, 2015; Sinha et al., 2005).

373 The assumption of a unique piedmont surface (piedmont fan surface) (Singh, 1996) at
374 the Himalayan scale is an oversimplification (Sinha et al., 2007), because fan deposition is
375 discontinuous and controlled by the balance between transport capacity and sediment supply.
376 Aggradation and incisional events occur when the Indian monsoon intensifies or decreases (Dey
377 et al., 2016). Landforms that originated in major humid climate periods of reasonable duration
378 were related to widespread alluviation and planation, whereas fans linked to shorter climatic
379 events have smaller lateral extents and are alluviated above the previous, more planar
380 landforms, which are only locally preserved in the piedmont. Therefore, the inter-megafan
381 piedmont surface is diachronic and has variable ages, ranging from 24 ka (Vassallo et al., 2015)
382 to 4.8 ka (Thakur et al., 2007) in the western Himalayas, 90 ka (Gibling et al., 2005) to 4.8 ka
383 in the central Himalayas (Srivastava et al., 2003; Parkash et al., 2000), to 60 ka to 3.5 ka in the
384 eastern Himalayas [see section 4.2 and Appendix B: Supplementary data for a compilation of

the results of Goswami et al. (2019), Singh et al. (2016), Starkel et al. (2015), Kar et al. (2014), Kumar et al. (2010), and Guha et al. (2007)].

The fluvial deposits of the modern foreland basin are covered by soils, the development of which varies with local geomorphologic stability. Remnants of soils are preserved in uplifted zones, whereas soils are usually reworked in flooded lower zones (Pati et al., 2012). Changing the soil character is also controlled by decreasing the geomorphic slope down megafan surfaces away from the mountain front (Hartley et al., 2013).

Finally, inland/terminal fans develop in the modern foreland approximately 50–100 km south of the mountain front (Pati et al., 2015). Their distribution in the distal plain has been partly attributed to faulting activity along the E-W and NE-SW topographic break scarps (Pati et al., 2012). The latter could be associated with the reactivation of basement faults that delineate tectonic blocks characterised by fluvial anomalies (Jain and Sinha, 2005) and are too distant (more than 50–100 km) to be related to the frontal propagation of the Himalayan tectonic prism (e.g., Chalaron et al., 1995).

Some fans are strongly incised in the piedmont zone by tens of metres up to a hundred metres (Abrahami et al., 2018), and the origin (tectonic or climatic) is discussed in Sections 3.2 and 4.2.

2.3.3 Present-day deformation of the plain and the Churia range

Topographic measurements were undertaken in east/central Nepal nearly half a century ago (Jackson and Bilham, 1994), spatial geodetic measurements have been in progress over the entire Himalayan range for nearly 30 years (Dal Zilio et al., 2019; Bilham et al., 1997), and interferometry techniques have been tested since the beginning of the millennium.

The synthesis of global navigation satellite system (GNSS) measurements and their models suggests that the convergence in the Himalayas is expressed by the creep of the MHT beneath the northern Himalayas and by elastic deformation (e.g., Ader et al., 2012). Indeed, the

411 southern part of the MHT is locked between great earthquakes (e.g., Dal Zilio et al., 2019) and
412 the Himalayan elastic deformation is progressively attenuated towards the south and ends close
413 to the Himalayan front.

414 GNSS data indicate that the deformation of the foreland basin zone and the southern
415 part of the Himalayas is smaller than the level of detection of the GNSS data in this area (Bilham
416 et al., 2017). This level of detection is more than 0.5 mm/yr and 1.5 mm/yr for horizontal and
417 vertical GNSS data, respectively, owing to the high noise level of GNSS continuous time series
418 from the Himalayas, even after correction for monsoon loading effects and residual seasonal
419 signals (Mencin et al., 2016; Flouzat et al., 2009). Nonetheless, local deformation rates of
420 several millimetres per year have been inferred via interferometry techniques (Yhokha et al.,
421 2015; Bhattacharya et al., 2014) or local GNSS networks (Gupta et al., 2017; Mullick et al.,
422 2009). However, a critical analysis of these data shows a low level of confidence; Bhattacharya
423 et al. (2014) only found a significant Sar interferometry signal along the rivers, a location
424 suggesting that the signal recorded geomorphologic/hydrologic processes. Yhokha et al. (2015)
425 did not perform a quality analysis of the calculated persistent-scattered-insar ground
426 displacement field. The several-millimetre GNSS signal found by Gupta et al. (2017) was
427 related to a velocity estimated in an Indian-fixed frame, but the signal does not exceed the
428 uncertainty of the data if expressed in a frame fixed to the front of the Himalayas, because the
429 motion is probably linked by the clockwise rotation of the Brahmaputra Valley and Shillong
430 Plateau (Vernant et al., 2014). The shortening estimated at 4.2 ±1.5 mm/yr through the piedmont
431 of the Gorubathan recess (Mullick et al., 2009) could be related to the elastic deformation at the
432 Himalayan scale in a zone where the locked zone of the MHT is narrow (Vernant et al., 2014).

433 The levelling data of Jackson and Bilham (1994) were cited by most studies concerning
434 the present-day deformation of the Himalayas (Dal Zilio et al., 2019; Bilham et al., 1997).
435 Nonetheless, they were recorded during a period of very limited microseismicity, as evidenced
436 by seismological studies (Pandey et al., 1999), which is in disagreement with the slow events

437 below the foothills and piedmont zones. Finally, the vertical motion in the plain evidenced by
438 levelling was re-interpreted as groundwater withdrawal subsidence (Bilham et al., 2017), a
439 point that is discussed in Sections 3.2 and 5.3.

440 Even during a medium earthquake, such as the 2015 Gorkha earthquake, no significant
441 motion affected the piedmont and frontal part of the Himalayas (Grandin et al., 2015). After
442 this earthquake, only the GNSS station located at Dhukuwa (Fig. 4) indicated a displacement
443 of a few centimetres of the MFT hanging wall, and no post-seismic deformation occurred in the
444 piedmont (Jouanne et al., 2019). Nonetheless, post-seismic creep processes may have affected
445 the easternmost part of the Himalayas during the 1947–1970 sequence of four earthquakes that
446 progressively ruptured the up-dip of the MHT (Bilham et al., 2017).

447

448 **3. The embryonic thrust wedge of the Birgunj area (east/central Nepal)**

449

450 3.1 The tectonics of the Birgunj-Hetauda area

451 In the Churia ranges of east/central Nepal, six MFT segments have been defined by
452 Divyadarshini and Singh (2019). Here, their nomenclature is used, although the studied zone
453 includes only the MFT2, MFT5, and MFT6 segments (Fig. 4). The evolution of the topographic
454 metrics between MFT5 and MFT6 indicates that the long-term uplift rate of MFT6 was greater
455 than that of MFT5 (Divyadarshini and Singh, 2019), suggesting that MFT6 cumulates the
456 shortening of MFT5 and MFT2 that merge close to Birgunj-Hetauda road (Mugnier et al., 2017)
457 (Fig. 4). In the Hetauda area, a tight asymmetric anticline with a steep southern flank is exposed
458 in the Middle Siwalik sediments just north of the MFT, forming the topographic front of the
459 Churia range. This is interpreted as a fault-propagation fold (Wahyudi et al., 2021) located at
460 the hanging wall of an intermediate décollement (Leturmy, 1997). A deeper décollement at the
461 base of the Lower Siwaliks is evidenced eastward (Lavé and Avouac, 2000) and the MDT
462 branches on this décollement (Schelling et al., 1991). A piggyback basin (Chitwan-Hetauda

Dun) is located above this décollement north of the frontal anticline and is delimited northward by the MDT (Fig. 4).

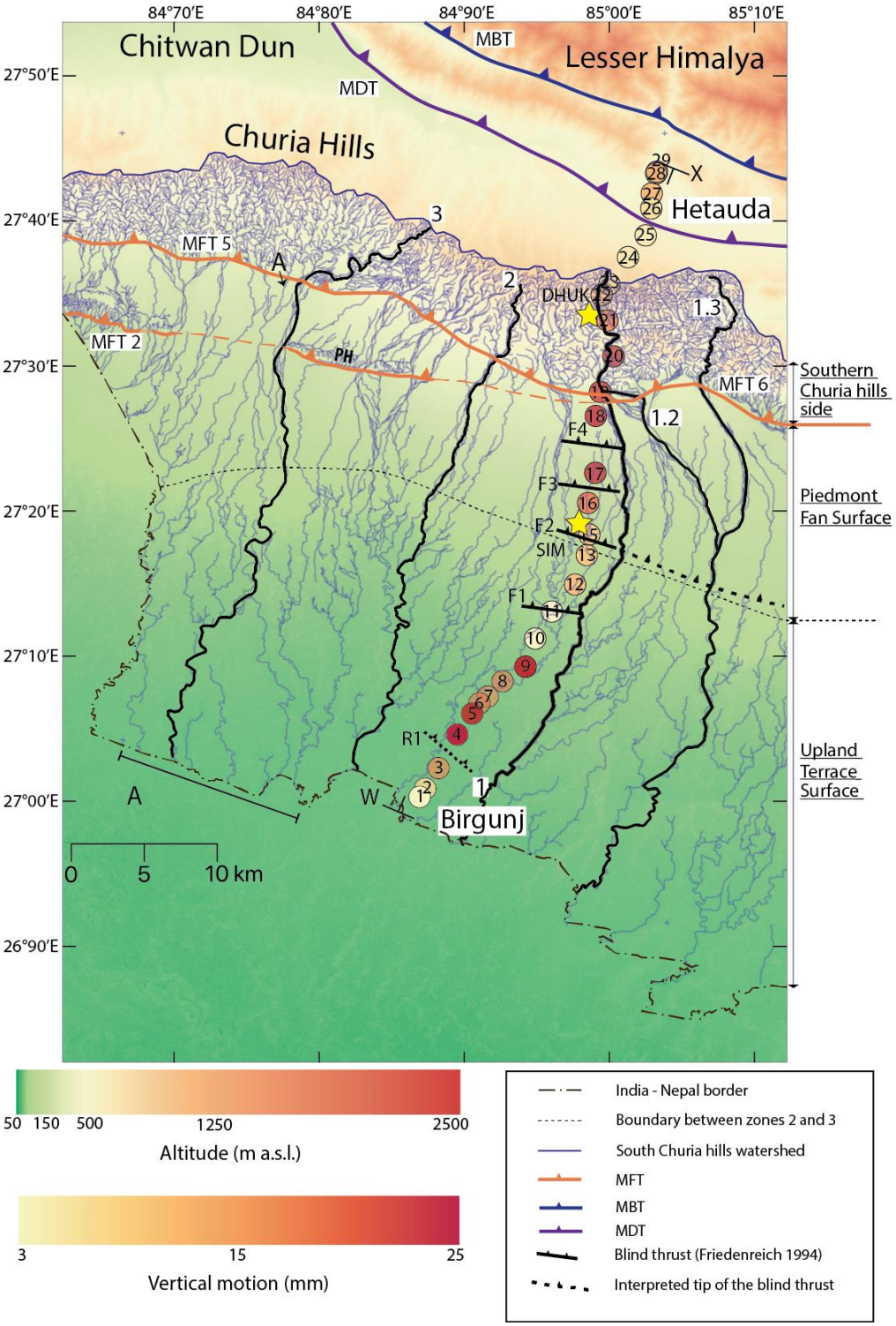

Figure 4: Structural and hydrological map of the Himalayan piedmont in the Birgunj area. The highlighted rivers 1, 1.2, 1.3, 2, and 3 refer to the profiles of Figure 6. MFT: Main Frontal Thrust; MDT: Main Dun Thrust; MBT: Main Boundary Thrust; PH: Parsa Hills; DHUK and SIM: Dhukuwa and Simra GNSS stations, respectively. The MFT location was obtained from Divyadarshini and Singh

(2019) and Mugnier et al. (2017). The altitude (a.s.l.) was obtained from the ASTER (2011) Digital Elevation Model. The drainage network was extracted from 1:25,000 topographic maps of the Nepal government. The numbered dots refer to the levelling sites along the Birgunj-Hetauda road (Jackson and Bilham, 1994). Their vertical motion relative to Birgunj is shown with a colour coding ranging from yellow (1 mm) to heavy red (28 mm). W-X: the location of Figure 5.

Beneath the piedmont, the seismic line 31ext (dots 9–29 in Fig. 4) suggests that several thrusts with spacing less than 10 km branch on the basal décollement at the base of the Tertiary wedge (Fig. 5) (Bashyal, 1998; Friedenreich et al., 1994; DMG, 1990). The elevation difference between the beds at the anticline axes and in the undeformed foreland is of the order of a few hundred metres. Thrust F2 (Fig. 5C) is clearly imaged, whereas the details of the other faults are poorly documented, and their offsets are difficult to quantify. These structures south of the MFT are considered in the following as an embryonic thrust wedge (Gonzalez-Mieres and Suppe, 2011).

Seismic line 31 (dots 1–15 in Fig. 4) (DMG, 1990) suggests reactivation of a basement fault (R1) (Fig. 5C) that forms the southern boundary of the Vindhyan graben.

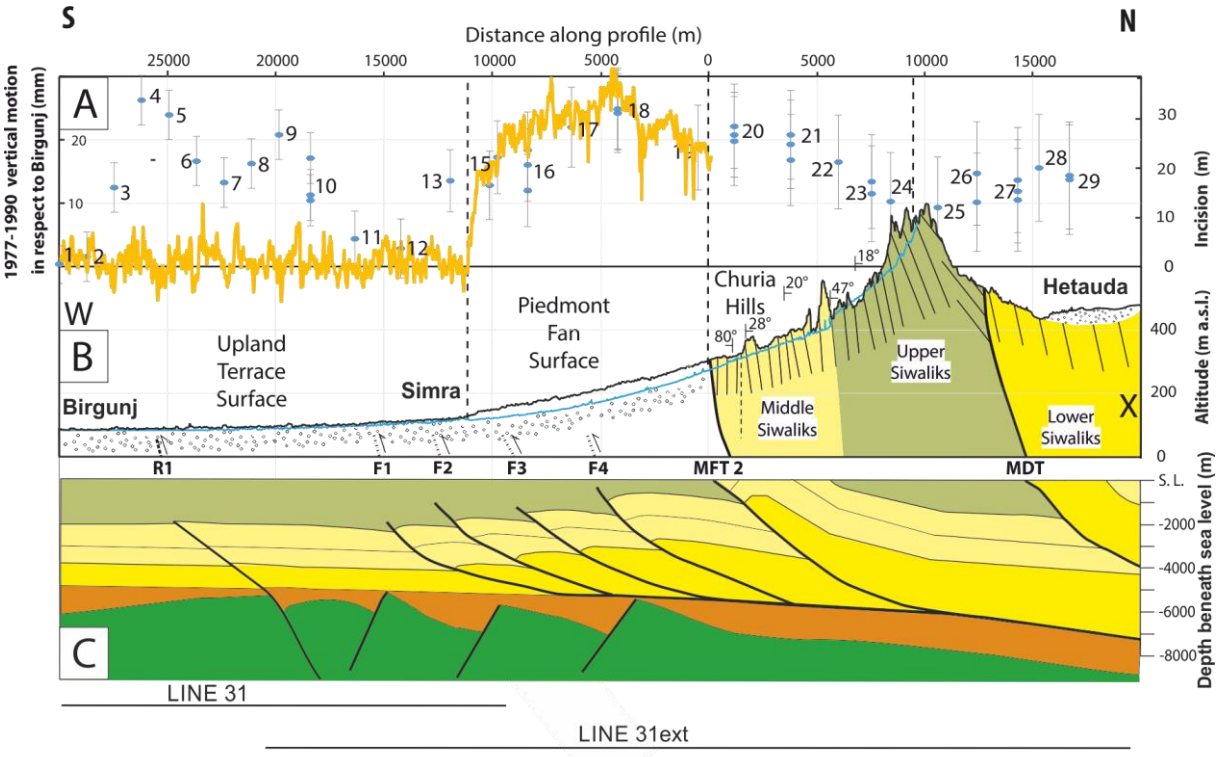

Figure 5: Comparison among incision, 1977–1990 vertical motion from levelling data, topographic profile through piedmont, river profile, and tectonic structures. The horizontal scale is similar for A, B, and C. (A) River incision (yellow line) and 1977–1990 vertical motion in the Birgunj area (blue dots) (Jackson and Bilham, 1994). (B) The black and blue lines represent the piedmont profiles (W-X on Fig. 4) and river profiles (river 1 on Fig. 4), respectively. The surface dips of the Siwalik strata were obtained from Schelling et al. (1991). (C) Interpretation of seismic profiles. The MDT (Main Frontal Thrust), MFT (Main Frontal Thrust), and southernmost thrusts were obtained from Bashyal's (1998) interpretation of seismic line 31ext. The reactivated basement fault R1 data were obtained from Jackson and Bilham's (1994) interpretation of seismic line 31 (DMG, 1990). The horizontal and vertical scales are the same.

3.2 Morphology and incision of the piedmont

The Birgunj area lies in the piedmont between the Gandak megafan and Bagmati fan (Fig. 1A). The interfan surface is characterised by small rivers that do not presently cross the southern ridge of the Churia Hills and originate from its southern flank. Nonetheless, rivers would have crossed the MFT2/MFT5 frontal system until ~50 ka (Divyadarshini et al., 2020) because the MFT5 had propagated at that time towards the west (Divyadarshini and Singh, 2019), leading to the capture of the Chitwan Dun drainage system by the Narayani/Gandak River (Fig. 1). This capture led to a major reorganisation of the drainage of the Birgunj piedmont, and the old piedmont fan surface recognised along with transverse profiles 1, 1.2, and 1.3 (Fig. 6) in this area could be abandoned due to this reorganisation. In contrast, the younger upland terrace surface that aggraded above the old piedmont fan surface could be related to the last 3.5–9 ka aggrading event (Srivastava et al., 2003, and other references in Appendix B).

The boundaries between the Southern Churia Hills, Piedmont Fan Surface, and Upland Terrace Surface morphologic zones (Srivastava et al., 2003) have been mapped in the area (Fig. 4) using the individual channel type changes, namely, braided, meandering, or straight

(Schumm, 1985), because a change in channel pattern is a subtle indicator of a slope change (Miall, 2013; Schumm and Khan, 1972). The northern zone displays small converging dendritic drainage systems corresponding to the southern Churia Hills, ranging from 400 to 800 m a.s.l. On the piedmont fan surface, rivers become more linear, with locally braided channels, as the altitude decreases to ~150 m a.s.l. through a slightly convex south-facing slope of 1.22 ± 0.05° to 0.63 ± 0.05°. The boundary between the piedmont fan surface and the upland terrace surface correlates with a change from a generally slightly convex area (1.22°–0.63°) to a nearly planar and very gently dipping (0.15°–0.11°) area (Fig. 6). Nonetheless, river profile 2 showed a strong slope variation (~1°) from a nearly planar piedmont fan surface to a nearly flat upland terrace surface. Finally, numerous small streams develop on the Upland Terrace Surface and create a dendritic pattern between the largest rivers that become slightly more sinuous.

Knickpoints affect the profiles of the rivers crossing the topographic front (Divyadarshini and Singh, 2019), but it is difficult to determine their origin. They could indicate changes in lithology or locations of active faults (Hack, 1973; Keller and Pinter, 2002), because the thrusts most often place distinct lithologies in contact with older and more indurated rocks in the hanging wall compartment. The major knickpoints in the Churia Hills (Fig. 6) could also be relics of knickpoints related to MFT surface ruptures that migrate upward (Cook et al., 2012). Finally, knickpoints in the piedmont could be located where the rivers split into an anastomosed system (river profile 1.2, Fig. 6).

A general anastomosed system developed south of the mountain front. West of the Birgunj-Hetauda road (Fig. 4), all the funnel-shaped geometries issued from the hill/plain boundary are interconnected, and the outlets at the hill/plain boundary, such as River A (Fig. 4), are finally distributed at the Nepal/Indian border in more than four rivers within a large 10-km zone. The anastomosed system is less extended east of the Birgunj–Hetauda road, although rivers 1, 1.2, and 1.3. (Fig. 4) are interconnected.

The large-scale anastomosed pattern to the west of the Birgung-Hetauda Road could be linked to several avulsions triggered by extreme monsoon floods (Makaske, 2001).

Nonetheless, anastomosed river systems can form when the base level is increased by a localised uplift zone (Grimaud et al., 2017; Makaske, 2001), and the river splits occurring around the Siwalik Hills of Parsa (Fig. 4) are probably linked to moderate MFT2 tectonic activity (Burbank and Anderson, 2011).

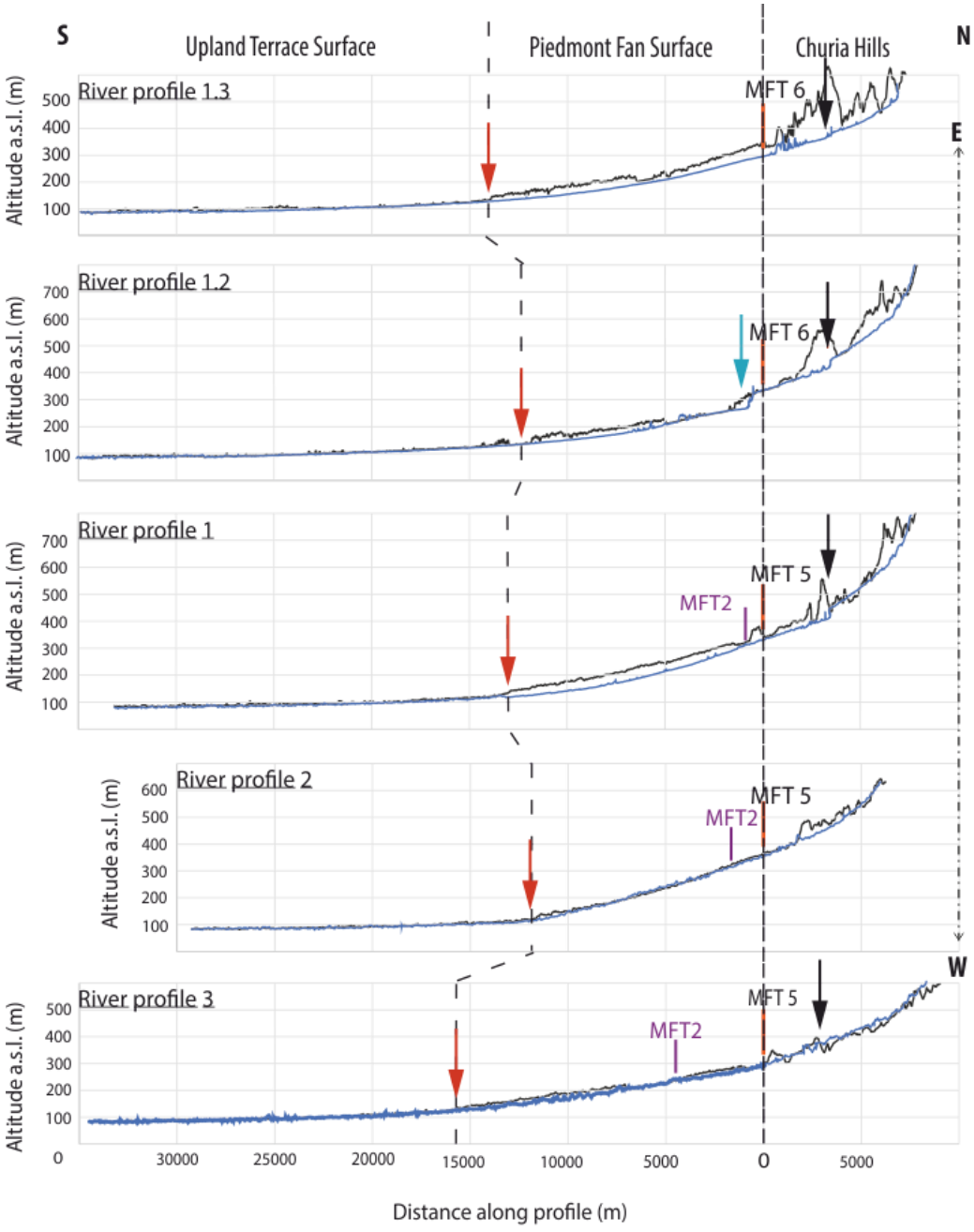

Figure 6: River (blue lines) and terrace (black lines) profiles from the southern flank of the Churia Hills (location in Fig. 4). The MFT5 and MFT6 locations are vertically aligned. MFT2 is indicated in purple. Black arrows show knickpoints in the Churia Hills. The blue arrow indicates the greatest knickpoint located south of the MFT. The red arrow indicates a noticeable break in the river slope.

552 The eastern part of the piedmont fan surface (profiles 1.3 and 1) (Fig. 6) shows an
553 approximate 20–40 m incision. As the sizes and topographic metrics of the catchments in the
554 Churia Hills are similar for all the rivers of the studied area (Divyadarshini and Singh, 2019),
555 sediment delivery is probably similar. Therefore, the greater incision of the eastern piedmont
556 could be related to the greater uplift. Along river profile 1, an incision of up to 40 m occurred
557 with respect to the adjacent terrace (Fig. 5B). In this particular case, the incision only furnishes
558 a minimum bound for the uplift (Vignon et al., 2017), because the aggradation occurring in the
559 upland terrace zone induces an increase in the relative base level, and the river slope probably
560 increases as a result of decreased flow associated with the capture of the upstream portions of
561 the watersheds by the Narayani River (Divyadarshini et al., 2020). Assuming that the old
562 piedmont surface was deposited close to, and possibly before, ~50 ka (Divyadarshini et al.,
563 2020), the 40 m incision suggests that the uplift rate affecting the piedmont is weak, less than
564 0.8 $mm \cdot yr^{-1}$.
565
566 The change in elevation between 1977 and 1990 was estimated using spirit levelling
567 (Jackson and Bilham, 1994) (Fig. 5A) and reached 28 mm with respect to Birgunj. A
568 comparison between incision and reiteration of the levelling profiles indicates that no incision
569 affects the morphology of the plain south of Simra (Fig. 4), where levelling reiteration shows
570 that the plain has risen (points 4-9) relative to the Birgunj (points 1-3) and Simra (points 10-15)
571 areas (Fig. 5A). This comparison supports the re-analysis of the levelling data by Bilham et al.
572 (2017), which suggests that two zones underwent subsidence due to recent (few tens of years)
573 and intense groundwater withdrawal in the vicinity of the Birgunj and Simra settlements, and
574 that the intermediate zone (point 4-9) remained stable, with no tectonic uplift during the
575 considered period.
576
577
578

3.3 Estimation of the deformation rates from deep structure geometry and relief development

The upper Siwalik units were deposited but thinned above the hidden structures, and the uplift rate at the hanging wall of these structures was thus lower than the deposition rate in the foreland (Fig. 5). The long-term subsidence of the foreland basin in central Nepal was ~0.4 $mm \cdot yr^{-1}$ over the last 10 Ma, according to the Raxaul drilling located south of Birgunj (Srinivasan and Khar, 1996; Sastri, 1979), and the short term deposition rate in the plain was estimated to be 0.6 $mm \cdot yr^{-1}$ to 1.4 $mm \cdot yr^{-1}$ for the few last millenniums (Sinha et al., 1996). Therefore, the uplift rate at the hanging wall of the hidden thrust structures was less than 1.4 $mm \cdot yr^{-1}$. Despite significant uncertainties, these values are one order of magnitude lower than the uplift rate estimated to be 15 ± 2 $mm \cdot yr^{-1}$ at the hanging wall of the MFT in the east-central Himalayas (Lavé and Avouac, 2000).

The shortening rate in thrust belts can be estimated using a simple and powerful method based on the conservation of volume. The excess area method is derived from the conservation of volume through the conservation of the surface in the cross-section (Goguel, 1952; Chamberlin, 1910) and is one of the more robust assumptions of quantitative structural geology (Moretti and Callot, 2012). The total horizontal shortening of a structure can be estimated by applying:

$$S = \Delta A / T_0, \qquad (1)$$

where T_0 is the initial (stratigraphic) thickness, ΔA is the excess area, and S is the shortening. This method, based on the estimation of two geometric quantities, is influenced by several assumptions and uncertainties. The uncertainty values indicated below for the excess area combine those for the current position measurement, initial position estimate, and volume change. The uncertainty values indicated for the initial thickness combine those for the measurement of the depth of the décollement level, the influence of the slope of the décollement level, and the deformation-related stratigraphic thickness change. Finally, the estimate of shortening is affected by the uncertainty that results from the propagation of all uncertainties

(details in Appendix C: Supplementary Data).

In the case of the Birgunj profile, the initial stratigraphic thickness T_0 of the Middle and Lower Siwaliks series is estimated from field work (Lavé and Avouac, 2000; Harrison et al., 1993) and from the Raxaul drill hole (Sastri, 1979) and is 2.8 ± 0.6 km. The excess area ΔA (Fig. 7) is 16.9 ± .32 km^2, leading to a 6 ± 1.5 km shortening.

The seismic lines had poor resolution, and most of the reflections were very tenuous. However, some of them would suggest onlaps above the top of the Middle Siwaliks (Friedenreich et al., 1994), thus indicating the activity of the hidden structures during the Upper Siwalik deposition. The beginning of the latter is estimated to be 1.8 ± 0.5 Myr in west/central Nepal (Gautam and Rösler, 1999) and 2.8 ± 0.5 Myr in eastern Nepal (Ojha et al., 2009). Considering the 6 ± 1.5 km shortening estimated from the excess area method, the long term (millennium to million-year scale) shortening rate distributed in the hidden belt would be 2.6 ± 1.3 $mm \cdot yr^{-1}$. The uncertainty of this estimation is large, but the shortening rate in the hidden belt is nearly one order lower than that in the Churia belt, estimated to be 21 ± 1.5 $mm \cdot yr^{-1}$ (Lavé and Avouac, 2000).

A method based on the adaptation of Eq. (1) (Epard and Groshong, 1993) was developed to link relief growth and incremental shortening in embryonic thrust belts (Gonzalez-Mieres and Suppe, 2006). In the case of a deformed and incised terrace, the surface of the deformed terrace refers to the final state, whereas the present-day river profile indicates the initial state because the present-day river profile is assumed to be the same as the palaeo-river profile when the terrace was abandoned at the end of its deposition. The increment of relief growth ΔAr (Fig. 7A) was estimated from the difference between the terrace profile and the river profile, that is, by summing the incision of the terrace along the cross-section, and the initial thickness (T_{0r}) is the thickness of the embryonic thrust wedge at its back. In the case of the Birgunj profile, the old piedmont surface is not defined north of the MFT, and ΔAr cannot be estimated above the inner part of the embryonic thrust belt located beneath the MFT. Therefore, the calculation, in

632 which $\Delta Ar = 0.43 \pm 0.3$ km^2 and $T_{0r} = 5.2 \pm 0.6$ km, underestimates the shortening with a value
633 of 83 ± 58 m, or 1 ± 0.8 mm·yr^{-1} during 50 to 115 ka.

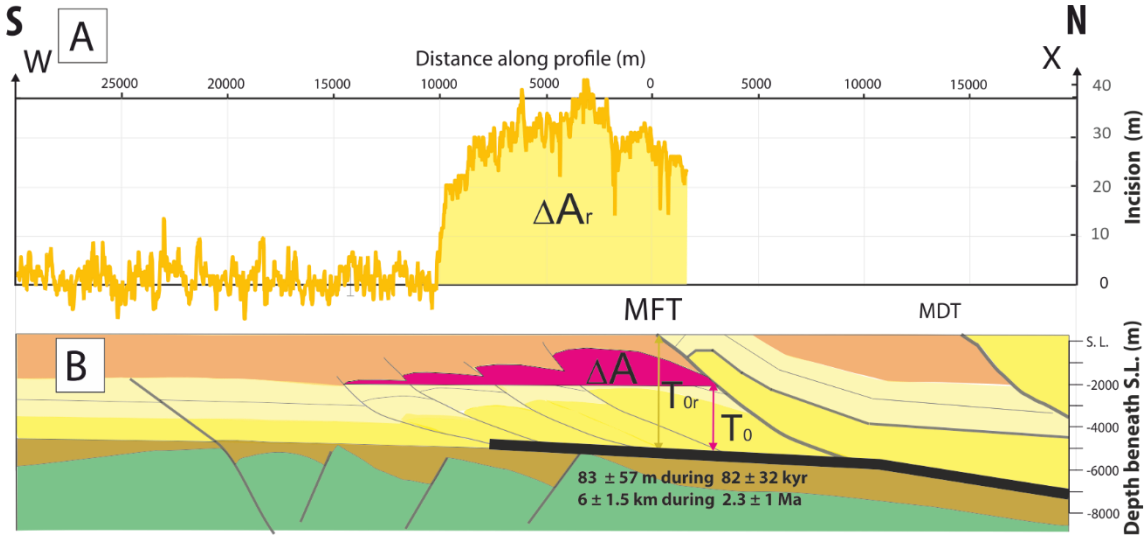

634

635 *Fig. 7: Estimated excess areas and initial thickness for the Birgang cross section [See Figure*
636 *S1 in Appendix C: Supplementary Data for details of assumptions made when applying the*
637 *excess area method (Chamberlin, 1910) and the area relief method (Gonzales-Mieres and*
638 *Suppe, 2006)]. . A) Relief areas created during the deformation of the old piedmont surface*
639 *(yellow zone: $\Delta Ar = 0.43 \pm 0.3$ km^2). B) Location on the interpreted seismic line of the*
640 *detachment (thick black lines) and of the excess area (red shaded zone; $\Delta A = 16.9 \pm .32$ km^2)*
641 *defined from the Upper to Middle Siwalik boundary. The initial thickness of the Lower and*
642 *Middle Siwaliks above the décollement and the thickness of the embryonic thrust belt at the*
643 *vertical of the MFT are $T_0 = 2.8 \pm 0.6$ km and $T_{0r} = 5.2 \pm 0.6$ km, respectively. Slip values*
644 *inferred along the detachment at the kilo-years and million-years refer to the application of the*
645 *excess area with respect to the old piedmont surface, and to the Upper to Middle Siwalik*
646 *boundary, with a décollement at the base of the Lower Siwalik (see explanation in Section 3.4).*

647

648

649

650

651

4. The hidden thrust belt of Darjeeling (Siliguri zone, India)

4.1 The tectonics of the Darjeeling zone

In the Darjeeling area (Fig. 8), the Himalayan mountain front is sinuous, and the Dharan salient is separated from the Gorubathan recess by the main Gish transverse fault (GTF). The GTF is both a tectonic lineament that extends northward to southern Tibet (Mukul, 2010), and a lateral ramp that offsets the MFT and MBT at the hanging wall of the MHT.

The topographic front is alternatively formed by Siwalik foothills or Lesser Himalayan reliefs in contact with Quaternary alluvia, as Siwalik exposures are missing in the Gorubathan Recess (Gansser, 1983). The recess could have originated from transverse faults in the Indian shield (Mukul, 2010), and the absence of Siwaliks could be linked to the erosional control of the thrust wedge dynamics (DeCelles and Carrapa, 2021; Chalaron et al., 1995).

East of the GTF, various adaptations of the classical Himalayan thrust nomenclature have been proposed owing to the absence of the Siwalik (Srivastava et al., 2017; Mishra et al., 2016; Nakata, 1989). Herein (Fig. 8), the MBT is considered as the contact between the Lesser Himalayan rocks and Quaternary sediments and MFT1 and MFT2, as defined by Mishra et al. (2016). MFT1 is singular because it is a footwall splay of the MBT (Fig. 9) with clear eastern and western branch points that only deform quaternary fans and terraces (Nakata, 1989). Furthermore, its dip flips over at its eastern termination (Goswami et al., 2019) in relation to the transverse faults (Goswami et al., 2013). MFT2 also deforms Quaternary sediments and is the emergence of historic seismic ruptures (Kumar et al., 2010). The Bharadighi fault is a back-thrust fault defined by Nakata (1989). The Batabari fault was inferred from the river morphology between the MFT2 and Bharadighi faults (Srivastava et al., 2017) and probably extends westward according to a passive seismic study (Large et al., in press).

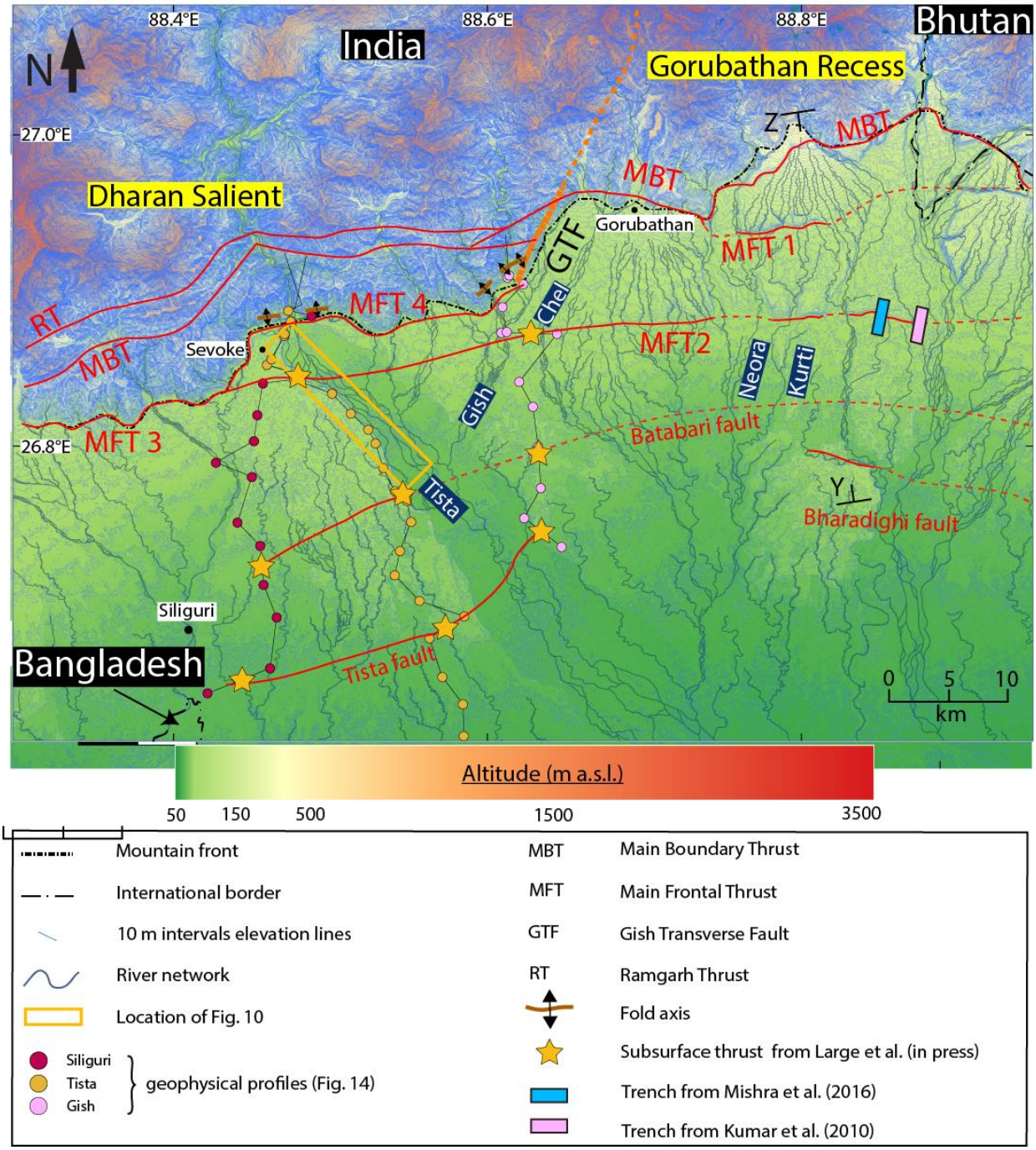

Figure 8: Map of the Siliguri area. Altitude from the ASTER (2011) Digital Elevation Model. River network extracted from satellite images (Maxar technologies). The Gish Transverse Fault (GTF) separates the western Dharan Salient from the eastern Gorubathan Recess and is indicated by the orange line. Thrusts (MFT: Main Frontal Thrust; MBT: Main Boundary Thrust; RT: Ramgarh Thrust; Tf: Tista fault) are represented in red. Z-Y stand for the location of Fig. 9. The yellow rectangle stands for the location of Fig. 10.

West of the GTF, the frontal structure above the MFT is mainly formed by a Middle Siwalik anticline with a narrow south flank that dips ~ 60° to the south and a gentle dip to the

north flank (Taral, 2017). Three distinct segments of the MFT were defined based on their branch patterns. MFT2 is imaged south of the front beneath the piedmont by three passive seismic profiles (Large et al., accepted) and is in the continuity of the fault trenched in the Gorubathan Recess (Mishra et al., 2016) (Fig. 8). It branches with the frontal structures at the transition between the MFT3 defined by Jayangondaperumal (personal communication) and the MFT4. The MBT and RT (Ramgarh Thrust) were defined by Mukul (2010), and the mapping of these thrusts close to the GTF was performed by Patra and Saha (2019). The Tista fault (Tf) and the west extension of the Batabari fault are inferred from the geophysical profiles located above the Tista megafan and the Gish River fan (Large et al., accepted). Tf is located ~20 km south of the morphologic front and induces a 200–400 m offset of the top of the Middle Siwaliks on the geophysical profiles (Large et al., accepted) (Fig. 10). Recent trenches suggest that the MFT3 has not been active for several thousand years (Jayangondaperumal, personal communication), whereas the late Quaternary alluvium of the Tista River onlaps the Middle Siwaliks and seals the MFT4 (Taral 2017). Thermoluminescence dating of fault gouges suggests that MFT4 and a splay of faults at its hanging wall were still active 40 kyrs and 20 kyrs ago, respectively (Mukul et al., 2007), whereas geomorphologic markers suggest that the MBT fault system is still active in the Dharan Salient (Mukul, 2000).

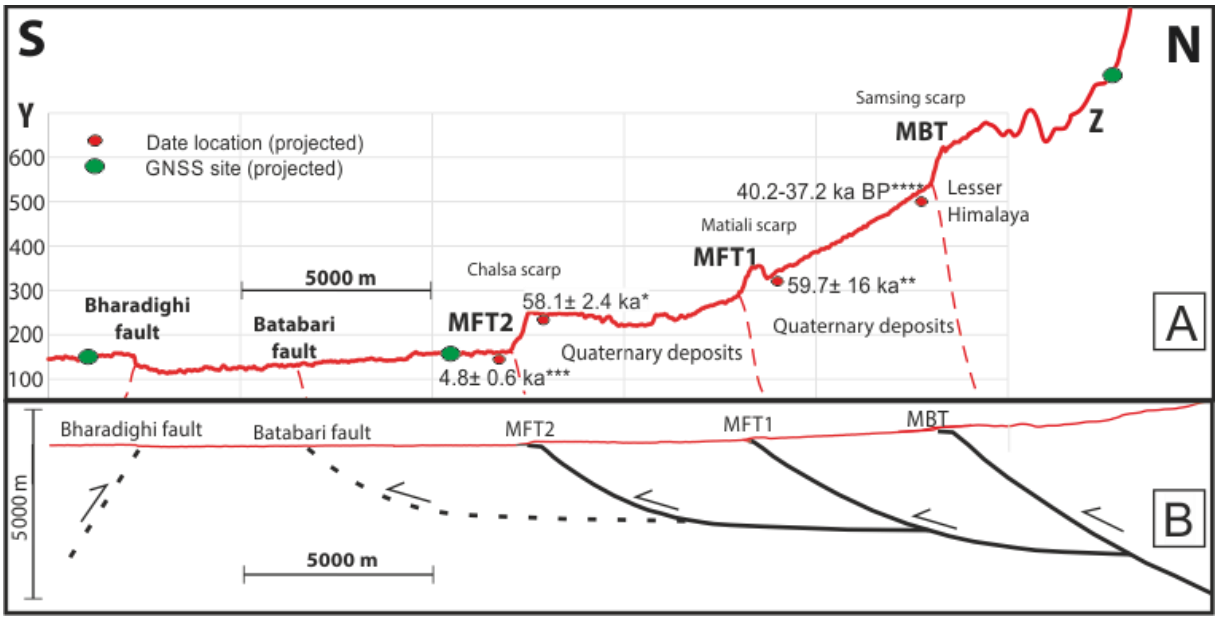

*Figure 9: Regional cross-section through the Matiali fan in the piedmont of the Gorubathan Recess (profile Y-Z on Fig. 8). A) Topographic profile (the vertical axis is magnified by 12) illustrating the location of the faults: Main Boundary Thrust (MBT) at the Samsing scarp and Main Frontal Thrust (MFT1) at the Matiali scarp and (MFT2) at the Chalsa scarp. Key datings were obtained from Starkel et al. (2015): *; Singh et al. (2016): **; Kar et al. (2014): ***; Guha et al. (2007): ****). The GNSS site was obtained from Mullick et al. (2009). The profile was constructed from the ASTER (2011) Digital Elevation Model. B) Deepest fault trajectories inferred for balancing procedures with no vertical exaggeration. See text and Appendix D: Supplementary data for the method.*

A small GNSS network of eight non-permanent sites was installed in Darjeeling (Mullick et al., 2009) and provided an estimate of the present-day deformation between December 2005 and March 2008. A significant extension is suggested across the Gish transverse fault, whereas in the Gorubathan Recess we found a 4.2 ± 1.5 mm/yr N-S shortening between the sites at the footwall of the MFT2 and at the hanging wall of the MBT, respectively (Fig. 9).

4.2 Morphology of the piedmont

Two types of river were observed in the Darjeeling piedmont. The first type originates north of the mountain front and has large catchments, such as the Tista, Chel, Neora, Murti, and Jaldhaka Rivers (Fig. 8). Most of these rivers incise the piedmont surface and display a braided pattern on the plain. The second type of river is located at the interfluves of the main rivers. These rivers originate south of the mountain front from palaeo-fans developed by the main rivers (Fig. 8) or, like those close to Gorubathan city, from smaller piedmont fans (Nakata, 1989). These small rivers display a radial drainage pattern on piedmont fans and are deflected across faults. These small and some of the large streams show an increase in the channel sinuosity and often develop a meandering pattern with well-developed scroll bars as they cross the piedmont zone and enter a low-gradient alluvial plain 18–25 km south of the mountain front. The evolution of the piedmont in this area is punctuated by a clear succession of incision-

731 deposition events in relation to variations in stream power and sedimentary supply during
732 climate fluctuations (Dey et al., 2016). This succession led to the development of several
733 encased (Kar et al., 2014) and/or superposed (Kar and Chakraborty, 2014) sedimentary units
734 related to alluvial fans, fill terraces, or fill-cut terraces (Goswami et al., 2013).

735 In the Dharan salient, a large megafan developed from the deposition of material
736 transported by the Tista River and extended from the Himalayan front down to its confluence
737 with the Brahmaputra (Fig. 1). It is characterised by a very gentle slope (~0.5%), and its apex
738 is strongly incised from the mountain front 25 km downstream (Fig. 10A). The incision along
739 the Tista River reaches 37 m at the apex and starts at 3.7 ± 0.7 ka (Abrahami et al., 2018) at an
740 average rate of 10 ± 2.2 mm·yr^{-1} (Fig. 10B). The incision of the megafan is significantly faster
741 than the contemporaneous incision in the Himalayan belt, which is less than 2.5 mm·yr^{-1}
742 (Abrahami et al., 2018). The incised sediments were previously deposited above an
743 unconformity (Fig. 10B), with an average sedimentation rate of 0.19 ± 0.03 mm·yr^{-1} between
744 113.8 ka and 21.6 ka and 0.94 ± 0.10 mm·yr^{-1} after that time (Abrahami et al., 2018).

745

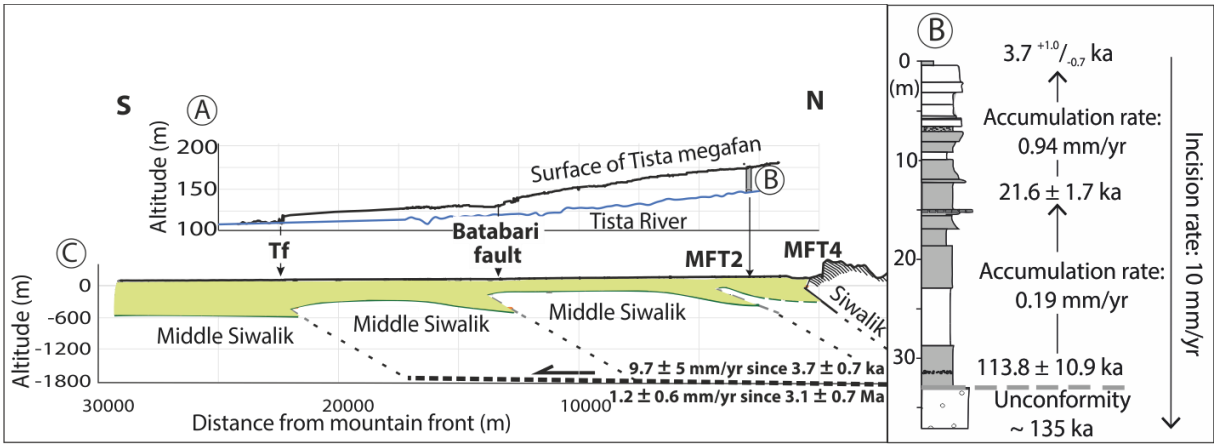

746

747 *Figure 10: Comparison of the incision of the Tista megafan and the underlying structures. A)*
748 *Topographic profiles of the Tista megafan and Tista River from Real-Time Kinematic Global Network*
749 *Satellite System data. B) Log of the late Quaternary sediments of the fan and inferred*
750 *sedimentation/incision story. (C) Inferred structures at depth from passive seismic profiles (Large et al.,*
751 *accepted) (western profile on Figure 8). The dashed line indicates the minimum depth of the base of the*

Siwalik group inferred from its stratigraphic thickness (Taral and Chakraborty, 2018) that is the probable location of the décollement. Thousand years and million years' time scale shortening rates are estimated in Sections 4.4 and 4.5, respectively. The details of the uncertainties calculation are detailed in appendix C: supplementary data. Tf: Tista fault; MFT: Main Frontal Thrust.

The surface elevation of the Tista megafan abruptly dropped by 9 ± 1 m at ~13 km and ~23 km downstream of MFT4 (Fig. 10A), forming steps that are located in the jungle and difficult to follow laterally. Nonetheless, they are interpreted as tectonic scarps because they are located above the Batabari and Tf structures (Fig. 10C), as evidenced by passive seismic records (Large et al., accepted). Therefore, much of the incision is related to localised fault-related uplift, whereas some is due to more distributed uplift or climatic fluctuations, as shown in Abrahami et al. (2018).

In the Gorubathan Recess, alluvial fans developed directly south of the mountain front. The compilation of 32 data ages and related mapping performed in the Gorubathan Recess area (Appendix B and location red pines in Appendix A: Supplementary data) suggests the deposition of three main sedimentary units (Fig. 11), the surfaces of which were abandoned at approximately 3.5–5, 37–40, and 58–60 ka, respectively. Another unit may have been abandoned at 23–28 ka (Singh et al., 2016, Guha et al., 2007).

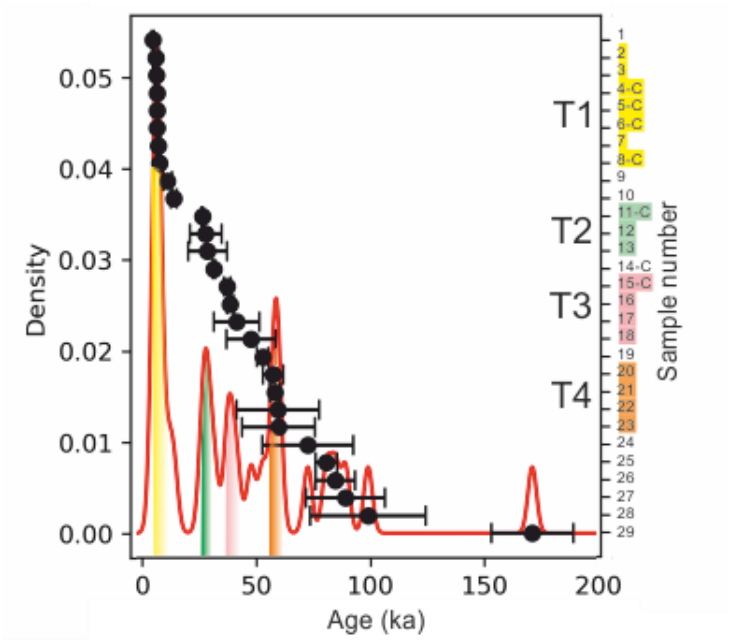

Figure 11: Age distribution of the sediment dated in the Gorubathan Recess. Individual data (numbers on right axis and black dots) from Goswami et al. (2019), Singh et al. (2016), Starkel et al. (2015), Kar et al. (2014), Kumar et al. (2010), and Guha et al. (2007), are presented in Appendix B: Supplementary data. Most of the data are obtained by Optically Stimulated Luminescence techniques. For the ^{14}C results (sample numbers with a '-c'), the ages have been calibrated using the Oxcal program (Ramsey, 2009) calibrated with the IntCal13 data set (Reimer et al., 2013). The common date used to mix Optically Stimulated Luminescence and ^{14}C results is 2020 AD. Density distribution (left axis and red curve) was obtained from the summation of individual probability distributions (Wegmann and Pazzaglia, 2009).

The 3.5–5 ka surface refers to the lower river terrace T1 (Nakata, 1989) and to large portions of the piedmont surface, while the 23–28 ka surface refers to a local river terrace T2. The 37–40 ka surface refers to a higher river terrace T3 encased in the Matiali fan (Singh et al., 2016), and 58–60 ka refers to the main surface of the Matiali fan (T4) (Fig. 12). The older units underlying the fans were dated between 80 ka and 171 ka. They are involved in the folds (Fig. 13) at the hanging wall of the faults, but their boundaries are difficult to precisely identify. Nonetheless, there is an unconformity between 135 ka and 114 ka in the Tista area (Abrahami et al., 2018) (Fig. 10C).

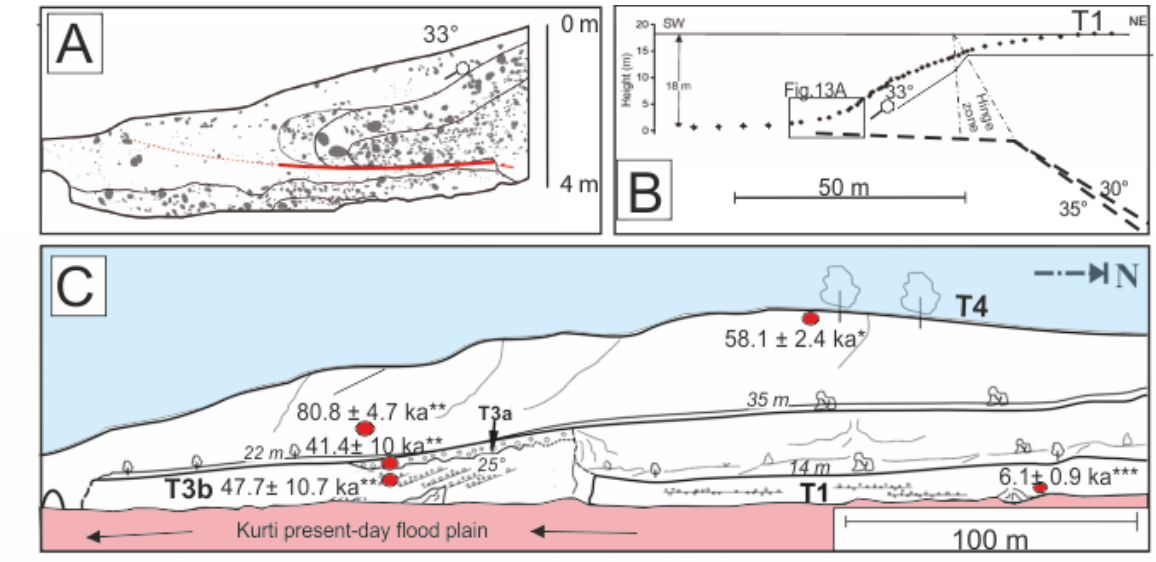

*Figure 12: Tectonic origin of the scarps and trenches in the Gorubathan Recess. A) Illustrative log of a trench through the MFT2 east of the Matiali fan (location on Fig. 8) showing an earthquake rupture that occurred before 1152 AD (Mishra et al., 2016). B) Topographic profile of the scarp affecting terrace T1 [adapted from Mishra et al. (2016)]. The inferred thrust geometry is based on the Jayangandaperumal et al. (2013) method. C) A tracing from a photograph showing the disposition of terraces north of the Chalsa scarp along the west bank of the Kurti River [adapted from Kar et al. (2014); location on Fig. 13A; dating location from Starkel et al. (2015): *; Singh et al. (2016): **; Kar et al. (2014): ***]. Shown are the elevations of the terraces T1 and T3 above Kurti River.*

The Matali fan is the most developed alluvial fan (Goswami et al., 2012) and is located between the Murti and Neora Rivers (Fig. 8). The size of the clasts decreased from megagravel in the apex part, with local blocks larger than 7 m, to finer pebble gravel and pebbly sand in the downstream part. The latest date is near the apex (Guha et al., 2007) and suggests that debris flows were still deposited at 40.2–37.2 ka cal BP and overlaid the older (~60 ka), finer-grained deposits characteristic of the rest of the Matiali fan. This fits with the initial interpretation of the two diachronic surfaces (Rangamati and Samsing surfaces) proposed by Nakata (1989). However, there are few dates from the different levels of the Matiali Fan, and we conclude that they only bracket the main period of growth of the fan from 37.2 ka to ~60 ka during the last glacial phase (Singh et al., 2016; Starkel et al., 2015).

Three steep south-facing scarps (Fig. 9A) offset the surfaces of the alluvial fan and the younger terraces (Goswami et al., 2013; Nakata, 1989). The scarps are located above tilted beds that are attributed from north to south to folding deformation over MBT, MFT1, and MFT2 (Srivastava et al., 2017; Kumar et al., 2010).

4.3. Fold and fault geometries

The detailed geometries of the faults and folds beneath the Matiali Fan and Tista megafan are poorly understood. The middle/upper Siwalik interface is characterised by faults and folds in the Tista area (Fig. 10). Analogous to the deformation imaged beneath the piedmont of the east-central Himalayas (Fig. 5C) (Bashyal, 1998), the upper sediments above the upper interface were syn-orogenic and were deposited above an embryonic thrust wedge that branched off the same deep décollement as the MFT (Figs. 10). In the area of the Matiali Fan, the style

of folding is considered by several authors to be related to fault-propagation folds (e.g., Guha et al., 2007; Srivastava et al., 2017).

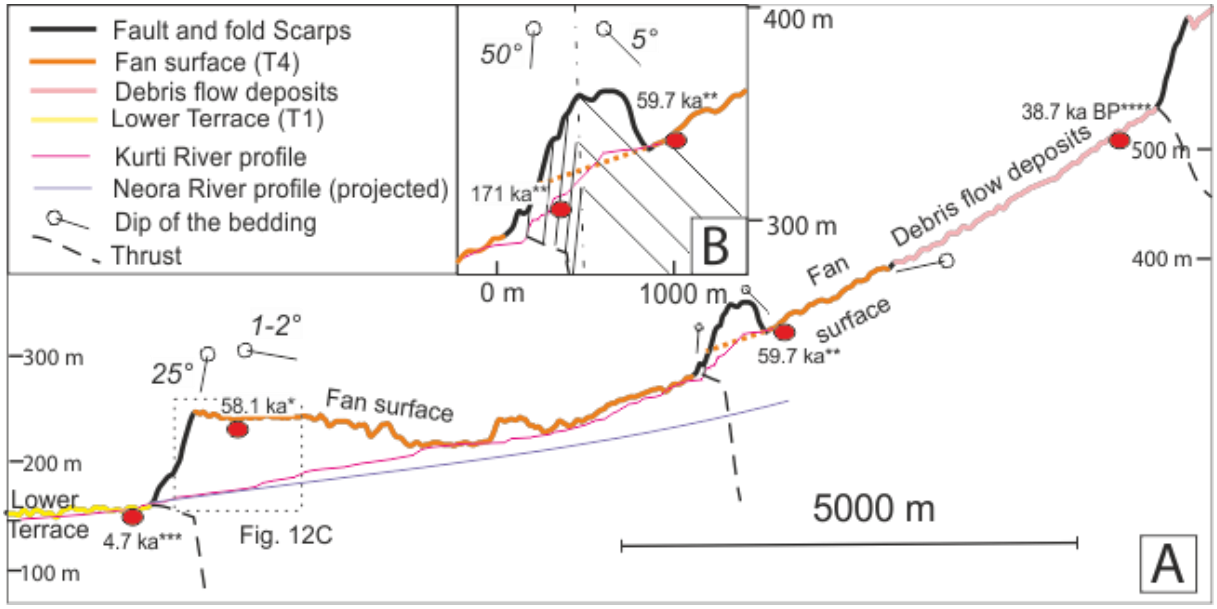

*Figure 13: A) Topographic profile through the Matiali fan illustrating the main surfaces, the scarps above the MBT (Samsing scarp), MFT1 (Matiali scarp), and the MFT2 (Chalsa scarp) and the location of key datings [from Starkel et al. (2015): *; Singh et al. (2016): **; Kar et al. (2014): ***; Guha et al. (2007): ****]. The profiles of the Kurti and Neora Rivers are projected on the cross-section to illustrate the incision. Profiles from the ASTER (2011) Digital Elevation Model. B) Magnified image of the Matiali scarp. The vertical scale is magnified by 12 in A) and B).*

An anticlinal structure is visible in the hanging wall of the western part of the Matiali Scarp (Das and Chattopadhyay, 1993; Nakata, 1989) (Fig. 13). Remnants of the fold were formed by mounds elevated at least 37 ± 12 m above the upstream Matiali fan surface and by the Matiali scarp offsetting the T4 fan surface, the offset of which was re-estimated from the DEM as 40 ± 10 m in the middle part of the fan (Kurti River) and 35 ± 10 m on the east bank of the Neora River.

The southern flank of the anticline is steeper than the slope of the Matiali scarp (30° on average) and dips southward by up to 50°, whereas the northern flank dips at a maximum of 5° to the north (e.g., Guha et al., 2007) (Fig. 13B). The stratigraphic thickness of the frontal limb of the anticline was at least 400 m (Das and Chattopadhyay, 1993). Therefore, the mounds are

remnants of a currently highly eroded fold, which is significantly higher than the mounds. This suggests that part of the development of the fold preceded the development of the scarp that offset the surface of the T4 fan.

The terraces deformed above the Chalsa Fault show an anticlinal fold with a progressively southward-tilted flank. In particular, the sediments beneath the T3b terrace were tilted more than the T3b surface, which was only slightly tilted (Fig. 12C). Bedding at the main scarp south of the T4 surface is difficult to observe, but Nakata (1989) indicated that it is steeper than the scarp slope. The T4 surface north of the scarp was weakly tilted to the north.

Field conditions make structural observations difficult, but a few trenches, made for construction (Guha et al., 2007) or paleoseismological studies (Mishra et al., 2016; Kumar et al., 2010) give clues to understanding thrust-fold relationships. Thrust was observed at the base of the Chalsa scarp (Mishra et al., 2016), suggesting that even if a fault-propagation fold could have initially developed, this fold is now cut and carried by the fault. The trenches excavated through the Chalsa Thrust (MFT2) show a nearly flat fault (Fig. 12A) (adapted from Mishra et al., 2016). However, a ramp is required to account for the 15–18 m uplift of the low T1 terrace a few tens of metres farther north (Fig. 13B), as well as for the more than 30° hanging wall tilting of the layers. Balancing methods (Jayangandaperumal et al., 2013) applied to T1 scarp geometry suggest that the ramp dips 30°–35° to the north.

Owing to the poor dataset on the faults beneath the Matiali Fan, their geometry can only be estimated using balancing procedures applied to the surface geometry of the scarps and deformed fan. This procedure is based on area conservation during landform development (Gonzalez-Mieres and Suppe, 2006), supplemented by equations linking uplift, fault dip, and shortening (Suppe, 2014). The analysis of the procedures (see Appendix D: Supplementary data) shows that the uncertainties related to the calculation of the décollement depth are mainly linked to the estimates of the excess area and dip at the upper part of the thrust ramp. The depths of the décollement linked to the Chalsa scarp (MFT2) and the Matiali scarp (MFT1) were then calculated between 2,300 m and 800 m and between 4,000 m and 1,000 m, respectively (see Appendix D: Supplementary data).

867 The stratigraphic thickness of the sediments in the foreland basin of this area is of the
868 order of a few kilometres (Karunakaran and Rao, 1976). Therefore, the depth of the décollement
869 associated with MFT2 north of the Chalsa scarp, although affected by a large uncertainty,
870 appears to be consistent with a décollement close to the base of the syn-orogenic sediment. For
871 MFT1, the depth of the detachment level is close to the thickness of the foreland basin sediment.

872

873 ### 4.4 The active tectonic rates affecting the piedmont at a scale of 10,000
874 years

875 When fault geometry is poorly understood, the shortening rate can nonetheless be
876 estimated from the uplift rate using simple kinematic models. To estimate the uncertainty
877 associated with this approach, two end-member models are used. The vertical simple shear
878 model (Molnar, 1987) is the simplest kinematic ramp-flat model that links sliding (S_f) and uplift
879 (U) above a ramp to the dip (θ) of the ramp using Equation (2):

880 $$S_f = U / \tan \theta. \quad (2)$$

881 The kinematic ramp-flat model based on the preservation of the stratigraphic thickness
882 (e.g. Suppe, 1983), can also be reduced to a single equation that links sliding along a flat and
883 uplift above a ramp, using Equation (3):

884 $$S_f = U / \sin \theta. \quad (3)$$

885 For a given uplift and dip, a greater shortening value was obtained using the kink-like
886 model than using the vertical simple shear model. The uncertainties concerning the model
887 choice, uplift, fault dip, and timing of fault slip are analysed in Appendix C: Supplementary
888 data. The maximum and minimum shortening estimates were obtained using the smallest
889 estimate of the dip (20° from Almeida et al., 2018) in the kink-like model and the greatest
890 estimate of the dip (35° from Mugnier et al., 1999a) in the simple shear model. Therefore, we
891 estimated the shortening rate and its uncertainty for the following fault scarps:

892 - The offsets of the 3.7 ± 0.7 ka old surface of the Tista megafan by the MFT2 and
893 Batabari fault scarps are both 9 ± 1 m (Fig. 10A), resulting in a vertical throw rate of 2.7 ± 0.6
894 mm·yr^{-1}. For each fault, the slip rate transferred along the basal décollement is 4.9 ± 3.6 mm·yr^{-}
895 ^{1}, leading to a total shortening rate of 9.7 ± 5 mm·yr^{-1} for the thrust system beneath the Tista
896 megafan.

897 - For MFT2, at the trench performed by Mishra et al. (2016) close to the Matiali fan, the
898 offset of the 4.5 ± 1 ka regional T1 terrace is 18–15 m (Fig. 12B). Therefore, the uplift rate is
899 3.6 $^{+1.5}/_{-0.9}$ mm·yr^{-1} and the shortening rate is 7.3 ± 5 mm·yr^{-1}.

900 - For MFT2 at the Chalsa scarp of the Matiali fan (Fig. 9), the age of the T4 surface is
901 59 $^{+1.5}/_{-6.5}$ ka (Singh et al., 2016; Starkel et al., 2015). The latter was buried at the footwall of
902 the fault beneath the T1 terrace, and the minimum uplift was 80 ± 10 m. This leads to an uplift
903 rate of 1.4 ± 0.3 mm·yr^{-1} and a shortening rate of 2.8± 2 mm·yr^{-1}.

904 For the MFT1 at the Matiali fault scarp (Fig. 9), the vertical offset of the fan surface is
905 40 ± 10 m. Therefore, the uplift rate is 0.7 ± 0.2 mm/yr^{-1}, and the shortening rate since 58–60
906 ka is 1.4 ± 1.1 mm·yr^{-1}.

907 In summary, the development of scarps began earlier in the Matiali fan than in the Tista
908 megafan, but the shortening rates estimated with the balanced methods are affected by more
909 than 50% relative uncertainty and are only useful for estimating the order of magnitude of the
910 shortening. Since 3.5–5.5 ka, the shortening rate has been 8.5 ± 6.2 mm·yr^{-1} in the Darjeeling
911 piedmont, whereas the shortening rate for the piedmont was 4.2 ± 2.3 mm·yr^{-1} for the 5 ka to
912 60 ka period.

913

914 ### 4.5 The active tectonic rates affecting the piedmont at a million year scale

915 Subsurface structures down to depths of a few hundred metres have been explored along
916 three approximately N-S trending profiles in the Siliguri area (Large et al., accepted) using the
917 horizontal-to-vertical spectral ratio method (Nakamura, 1989 (Fig. 14) (location in Fig. 8). This

method only displays the major interfaces characterised by strong velocity contrasts and does not provide a detailed picture of the subsurface structures (Guéguen et al., 2007; Hinzen et al., 2004).

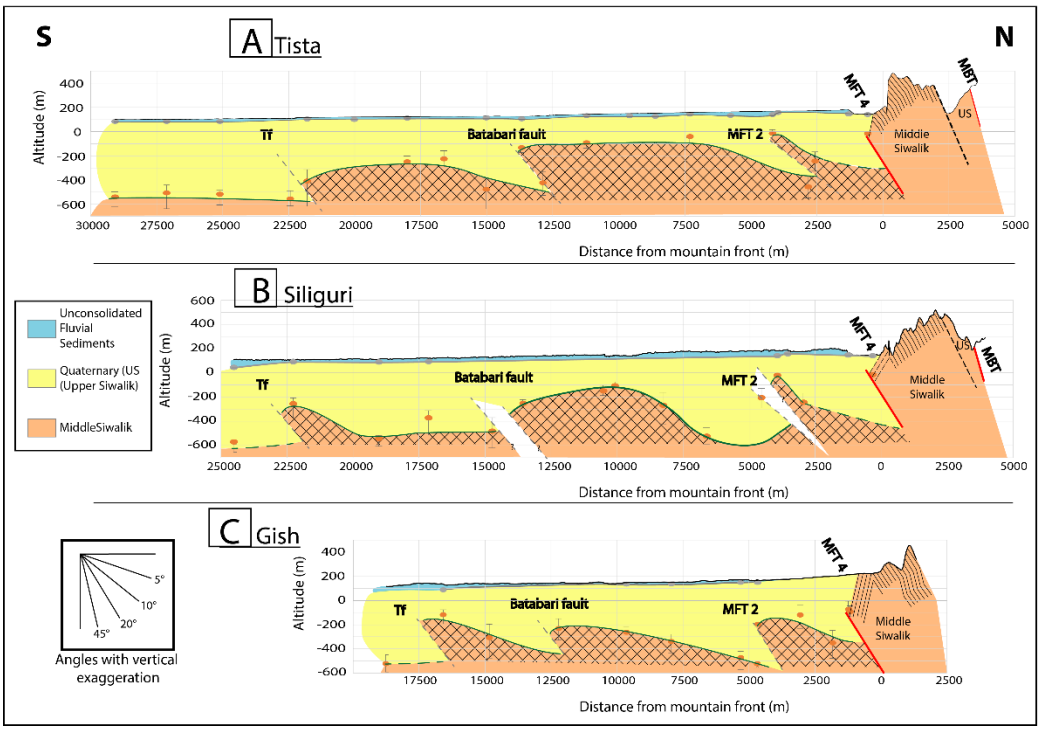

Figure 14: Interpretation of three profiles inferred from ambient seismic data in the Siliguri area (Large et al., accepted). Location of the profiles in Figure 8. The dips of the Siwalik strata along the Gish and Tista sections are from the data of the present authors and Acharyya et al. (1987). Green lines indicate the boundary between Upper Siwalik and Middle Siwalik sediments. Suggested thrusts are indicated by dashed grey lines. Gridded surfaces refer to the excess area surfaces, estimated at 6.6 ± 2.4 km^2, 6 ± 2.5 km^2, and 3.5 ± .51 km^2 for the Tista ([A]), Siliguri ([B]), and Gish ([C]) cross-sections, respectively. Note that the vertical scale is strongly exaggerated, and the bottom left inset indicates the real values of the fault dips. Tf: Tista fault; MFT: Main Frontal Thrust; Mbt: Main Boundary Thrust; US: Upper Siwalik.

The excess area method (Eq. 1) (Goguel, 1952) is well suited for estimating the shortening related to such imaged structures, because the method is insensitive to the details of the upper interface geometry. The interface between soft sediment and stiffer sediment is interpreted as the top of the Middle Siwalik rocks, the age of which is 3.1 ± 0.7 Ma (Chakraborty et al., 2020; Coutand et al., 2016), and the décollement is not deeper than the base of the Siwaliks. The ΔA values of the three cross-sections Tista, Siliguri, and Gish are 6.6 ± 2.5 km^2,

6 ±2.4 km^2, and 3.5 ± 1.5 km^2, respectively (Fig. 14). The maximum initial thickness T_0 was 1,800 ± 300 m in the Tista area (Taral and Chakraborty, 2018) and 1,300 ± 300 m in the Gish area (Chakraborty et al., 2020). The shortenings and uncertainties were calculated using Eq. 1 and Appendix C: Supplementary data. The shortening values are 3.7 ±1.5 km, 3.3 ± 1.5 km, and 2.7 ± 1.3 km (Fig. 14), respectively for the three cross-sections.

The difference between the three cross sections is not meaningful owing to significant uncertainties. The shortening is therefore considered to be 5.8–1.4 km and the mean shortening rate at the million-year scale is 1.1 ± 0.7 $mm \cdot yr^{-1}$. This long-term shortening rate was smaller than the short-term rate averaged at 3.7 ka (Section 4.4). This increase in velocity probably post-dated the last phase of sedimentation of the Tista megafan, which still occurred between 113.8 ka and 3.7 ka at rates close to the long term subsidence (Fig. 10B).

5. Summary

Our synthesis in both east-central Nepal and the Darjeeling piedmonts reveals that uplifted surfaces and/or drainage perturbations were observed 10–40 km south of the mountain front. Subsurface data strongly suggest that these morphological features are linked to the development of several thrusts and associated folds below the piedmont. The geometry and kinematics of these hidden structures forming 25–40 km south of the MFT and that branch off the MHT are summarised below.

5.1. Structural style beneath the piedmont of the Himalayas

The geometries obtained from the Himalayan piedmont illustrate the concepts of syn-sedimentary tectonic structures. The analysis of tectonic/sediment relationships provides simple and robust information about the uplift rates of the embryonic fold and thrust belt beneath the Himalayan piedmont (Fig. 15). In the case of syn-sedimentary thrusts above a décollement, the

geometry is classically interpreted with regard to the ratio (V_{sed}/V_{upl}) between the long-term sedimentation rate at the footwall (V_{sed}) and uplift rate at the hanging wall (V_{upl}) (e.g., Barrier et al., 2013; Bonnet et al., 2008). When the sedimentation rate is significantly higher than the uplift rate, evidence of tectonics at the surface remains limited (Fig. 15C) ('c' structure type in Table 2); however, sedimentation around the structures is disturbed and displays specific angular relationships (Almeida et al., 2018). When the uplift rate was close to the sedimentation rate, the hanging wall emerged slightly (Fig. 15B), and syn-kinematic sedimentation exerted a strong influence on the trajectory of emergent thrusts (Butler, 2020; Mugnier et al., 1997; Suppe, 1983), whereas tectonics greatly influenced the drainage pattern (Roy et al., 2021; Delcaillau et al., 2006). When the uplift rate was higher than the sedimentation rate, thrusts and their hanging walls emerged, footwall sediments were extensively sub-thrusted, and the hanging wall eroded (Fig. 15A) ('a1' structure type in Table 2).

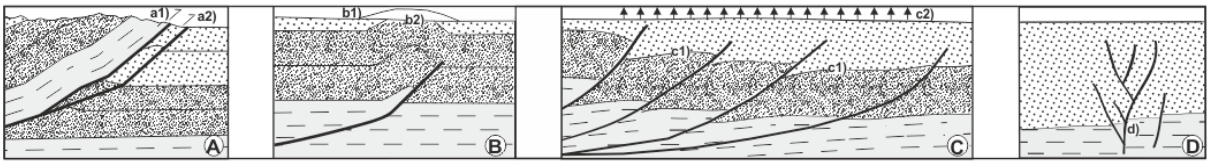

Figure 15: Typical syn-kinematic sediment/thrust relationships at the front of the Himalayas. (A) Emergent frontal thrust. The mean uplift rate is greater than the mean sedimentation rate; a1) thrusting of the Neogene Siwalik beds above the piedmont; a2) ruptures can locally occur along the footwall splay of the MFT and affect the piedmont. (B) Fault-related anticline. The mean uplift rate was close to the mean sedimentation rate; b1) emergent fault-related anticline (when the sedimentation is less than the uplift); b2) hidden fault-related anticline (sedimentation momentarily greater than the uplift). (C) Hidden thrust splay; c1) the long-term uplift rate is smaller than the long-term sedimentation rate; c2) a small change in the present-day surface is detectable. (D) Structural reactivation of basement fault. Examples of a1), a2), b1), b2), c1), c2), and d) are indicated in the right column of Table 2.

Finally, reactivations affected the steep basement structures beneath the foreland basin ('d' type of structure in Table 2). They can be characterised either by thrust or normal faulting; the latter is linked to the flexure of the lithosphere beneath the foreland basin (Duroy et al., 1989). However, a strike-slip component frequently occurs because most of the pre-existing

faults in the basement are oblique to the Himalayan structures (e.g., Godin et al., 2019; Mugnier et al., 2017), often resulting in flower structures in the overlying sediment pile (Fig. 15D) (Raiverman et al., 1994). For example, basement reactivations could explain the recent deformations highlighted by the inland/terminal fan alignments located along NW-SE fault scarps in the Ganga plain (Pati et al., 2012).

Thus, this analysis of the tectonic/sediment relationships provides a classification of the foreland and piedmont tectonic structures (Fig. 15), allowing for a better understanding of the variety of studied structures (Table 2).

5.2. Deformation rates in the piedmont of the Himalayas

All of the above quantifications lead to the following results (Table 3):

For the most recent period (less than 3.7–4.5 ka), values of 4.7 to 12.3 $mm \cdot yr^{-1}$ are consistent with both the Tista and Matiali shortening rates across the Darjeeling piedmont if uncertainties are taken into account. Furthermore, at least one of the shortening rates is between 2.3 and 14.7 $mm \cdot yr^{-1}$. Therefore, we estimated the shortening rate to be 8.5 ± 6.2 $mm \cdot yr^{-1}$ in the Darjeeling piedmont for this period.

For the long term (million years' scale), if uncertainties are taken into account, the 1.4 $mm \cdot yr^{-1}$ value is compatible with the shortening rates across the piedmont of the Birgunj and Darjeeling zones. Furthermore, at least one of the shortening rates is between 0.4 and 3.8 $mm \cdot yr^{-1}$. Thus, the shortening rate is estimated to be $1.4\ ^{+2.4}/_{-1}$ $mm \cdot yr^{-1}$ for the entire piedmont.

For the period covering a few tens of thousands of years, the rate of 1.4 $mm \cdot yr^{-1}$ in the Birgunj area is compatible with the estimated long time shortening (on a million-year scale). In the Matiali area, the shortening rate is more important, and this moderate increase in the mean shortening rate may be induced by the large increase evidenced in this area for less than 4.5 Ka recent period.

Table 3: Parameters used and estimates of the shortening rates at different time scales. The propagation of uncertainties related to the balancing procedures is detailed in Appendix C: Supplementary data.

Cross-sections	Figure	Age	Excess area	Initial thickness	Uplift	Uplift rate	Shortening	Shortening rate
Million years scale		**Ma**	**Km^2**	**km**			**km**	**$mm{\cdot}yr^{-1}$**
Birgunj	Fig. 7B	2.3 ± 1	16.9 ± 2	2.8 ± 0.6			6.0 ± 1.5	**2.6** ± 1.2
Siligury	FIG. 14B	3.1 ± 0.7	6 ± 2	1.8 ± 0.3			3.3 ± 1.5	**1.1** ± 0.4
Tista	FIG. 14A	3.1 ± 0.7	6.6 ± 2	1.8 ± 0.3			3.7 ± 1.5	**1.2** ± 0.5
Gish	FIG. 14C	3.1 ± 0.7	3.5 ± 2	1.3 ± 0.3			2.7 ± 1.3	**0.9** ± 0.5
Millenium yrs Scale		**ka**	**Km^2**	**km**	**m**	**$m{\cdot}yr^{-1}$**	**m**	**$mm{\cdot}yr^{-1}$**
Birgunj	Fig. 7A	82 ± 32	0.43 ± 0.3	5.2 ± 0.6			83 ± 56	**1.0** ± 0.8
Matiali (MFT2)	*Fig. 9A*	*56.5 ± 4*			*80 ± 10*	*1.4 ± 0.2*	*160 ± 114*	*2.8 ± 2.0*
Matiali (MFT1)	*Fig. 9A*	*56.5 ± 4*			*40 ± 10*	*0.7 ± 0.2*	*80 ± 60*	*1.4 ± 1.1*
Matiali (MFT2 + MFT1)	Fig. 9A	56.5 ± 4					240 ± 128	**4.2** ± *2.3*
East of Matiali (MFT2)	Fig. 12B	4.5 ± 1			16.5 ± 1.5	3.7 ± 0.9	33 ± 23	**7.3** ± 5.0
Tista (MFT2)	*Fig. 10A*	*3.7 ± 0.7*			*9 ± 1*	*2.4 ± 0.5*	*18 ± 13*	*4.9 ± 3.6*
Tista (Batabari F.)	*Fig. 10A*	*3.7 ± 0.7*			*9 ± 1*	*2.4 ± 0.5*	*18 ± 13*	*4.9 ± 3.6*
Tista (MFT2 + Batabari F.)	Fig. 10A	3.7 ± 0.7					36 ± 18	**9.7** ± *5.0*

5.3. A present-day deformation in the embryonic thrust belt?

Present-day deformation in the piedmont has been suggested in a few places, from the central Himalayas to the eastern Himalayas (Table 2) (Gupta et al., 2017; Yhokha et al., 2015; Bhattacharya et al., 2014; Mullick et al., 2009). Nonetheless, none of these studies showed a high level of confidence (see section 2.3.3).

The 1977–1990 levelling data of east-central Nepal (Jackson and Bilham, 1994) (Fig. 5A) have been used and mixed with the 1991–2015 GNSS data in most of the studies of the inter-seismic deformation of the Himalayas, since the pioneer work of Bilham al. (1997) to the

work of Dal Zilio et al. (2020). However, the mixing of data acquired during different periods and with different spatial distributions is difficult. Furthermore, this can be misleading because the levelling signal recorded in the piedmont was first interpreted as tectonic (Jackson and Bilham, 1994) before a re-interpretation of groundwater withdrawal subsidence (Bilham et al., 2017). Although historical levelling is non-reproducible owing to the disappearance of benchmarks, the hypothesis of groundwater withdrawal subsidence that would have continued to the present is testable. The Simra GNSS (SIM) permanent station (Fig. 4) has recorded a subsidence of 2.88 ± 1.1 mm/yr in the vicinity of the leveling profile since 1995 (Jouanne et al., 2017) and has not indicate significant horizontal motion with respect to the Indian plate (Jouanne et al., 2017; Ader et al., 2012), suggesting that the groundwater withdrawal subsidence hypothesis (Bilham et al., 2017) is the most plausible one.

While slow slip events are evidenced in many subduction zones around the world (Jolivet and Frank, 2020), there is no unambiguous geodetic or seismological evidence of such events in the Himalayas and its piedmont. The initial evidence of slow slip in east-central Nepal (Jackson and Bilham, 1994) was predicated by the perceived credibility of levelling data before the advent of precise CGPS data. Subsequent decades of geodetic studies in the Himalayas have been unable to confirm this inference, and their precision [~ 0.5 mm/yr (Mencin et al., 2016; Flouzat et al., 2009)] furnishes an upper bound for a hypothetical slow slip.

6. Discussion

The MFT is a piggyback transported by the embryonic thrust belt and, by definition, the motion along the MFT is out-of-sequence. Nonetheless, the main point is that the deformations of the hanging wall of the MFT and the embryonic thrust belt are synchronous at the Quaternary time scale but occur at very different rates (Fig. 16). The long term shortening rate is in the order of 20 $mm \cdot yr^{-1}$ for the Himalayan belt (Lavé and Avouac, 2000), whereas the shortening rate of the embryonic thrust belt is only $1.4^{+2.4}/_{-1}$ $mm \cdot yr^{-1}$ at the long term scale (Sections 3.3

and 4.5). Although the uncertainties are great, the deformation of the embryonic thrust belt is clearly slower (Fig. 16A) than the Himalayan belt deformation and is probably one order of magnitude slower.

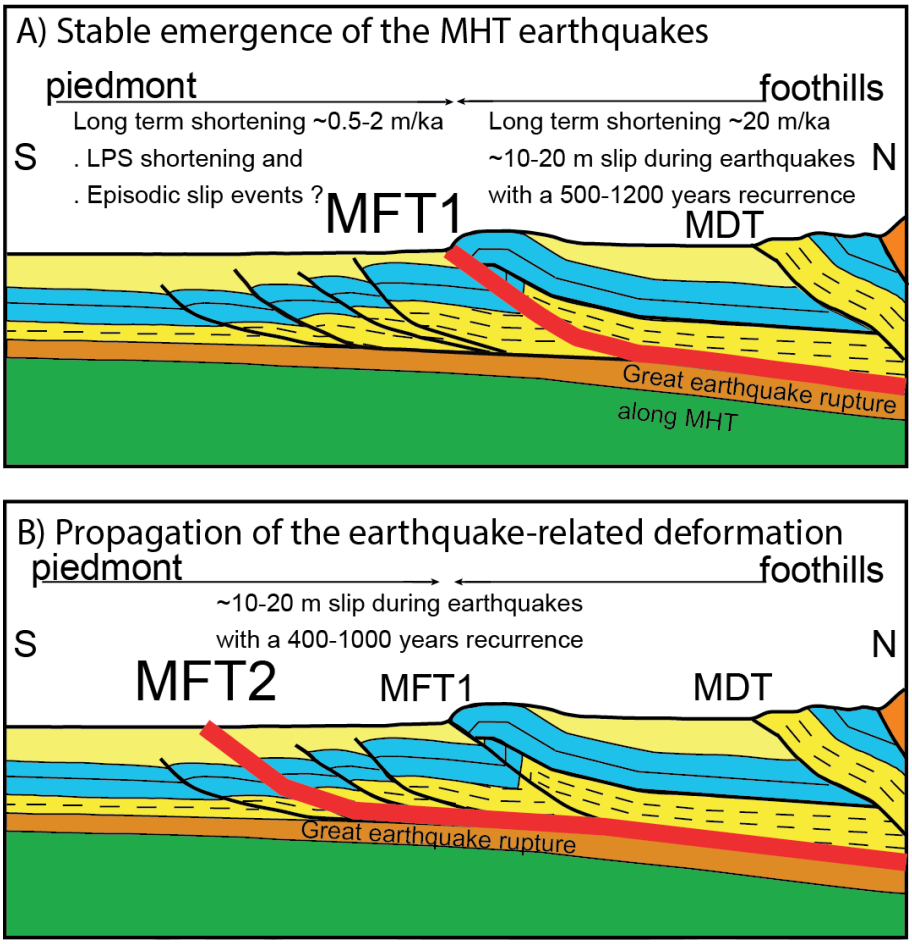

Figure 16: Schematic diagram of the contrasted deformation between the embryonic foreland belt and the faster hinterland uplifted belt. A) Stable emergence of the MHT earthquake events at the frontal structure (MFT1); B) forward propagation of the emerging MHT (MFT2): incorporation of the embryonic belt in the thrust belt.

These contrasting deformation rates agree with the findings in other mountain belts and accretionary wedges (Gonzalez-Mieres and Suppe, 2011), where the shortening is not currently concentrated in the morphologically elevated zones, but where embryonic thrust belts develop ahead of the thin-skinned thrust belt. In these embryonic zones, typical shortening rates are in the range of 0.1–3 mm·yr^{-1} and represent only 1–10% of the regional plate tectonic rates (2–6 cm·yr^{-1}) (Gonzalez-Mieres and Suppe, 2011).

No historical or instrumental data have recorded the growing structure or faulting during earthquakes in the embryonic thrust belt. Therefore, the deformation mechanism of the

embryonic thrust belt remains enigmatic and various hypotheses are discussed below.

A) A part of the long-term deformation of the Himalayan embryonic thrust belt could be large-scale horizontal pure shear shortening (LPS) (e.g., Weil and Yonkee, 2012; Mitra, 1994), which occurs ahead of a thrust belt prior to, or during, the earliest motion on a thrust. During the LPS stage, incipient large-scale (more than a kilometre) faults, folds, and smaller-scale deformation structures develop. At the front of the Taiwan thrust belt (Le Béon et al., 2019), the LPS stage combines small-scale buckle folds, contraction faults, compaction and internal shortening parallel to the layers. These small-scale processes could occur in the hidden thrust belt south of the Himalayas, but are not directly observable. The internal deformation evidenced in the beds of the Churia ranges (Fig. 2B) absorbs less than 7% of the total horizontal shortening (Srivastava and Mukul, 2020) and could be partly related to such an embryonic stage. Furthermore, the geometry of the axial surfaces of the frontal folds (Almaida et al., 2018) (Fig. 3B) suggests a shearing above the décollement (Suppe et al., 2004). As GNSS does not detect a present deformation, any steady-state penetrative deformation rate would have to be smaller than the 0.5 $mm \cdot yr^{-1}$ GNSS precision. Then, the strain rate in the embryonic thrust belt would be less than $1.5.10^{-15}$ s^{-1} if such a shortening rate is distributed along a 10 km long structure, which is in agreement with the common strain rates averaged over long-term geological times (Fagereng and Biggs, 2019).

B) The long-term deformation rate and short-term deformation rate in the piedmont are $1.4\ ^{+2.4}/_{-1}$ $mm \cdot yr^{-1}$ and < 0.5 $mm \cdot yr^{-1}$, respectively. Although the uncertainties are large, deformation with an episodic character is probably necessary to reconcile a long-term deformation of a few $mm \cdot yr^{-1}$ with nearly null instantaneous deformation. The time scale and origin of such episodic deformations are not yet known, and many scenarios have been proposed. Thus, hypotheses such as large earthquakes, comparable to the 1934 earthquake, which would propagate under the piedmont with a recurrence on the order of 10 millennia (Duvall et al., 2020), or moderate slips of a few tens of centimetres with a hundred-year recurrence cannot be excluded. The dissipation of post-seismic stresses in small events, which would follow great events occurring

along the MHT and MFT, is an issue that should be explored because the stresses associated with the rupture of the great Himalayan earthquakes are probably the primary forces responsible for the southward growth of the Himalayas.

C) Nonetheless, great earthquakes rupture in the Darjeeling piedmont of the Himalayan chain, as in the case of the Matiali fan (Fig. 12B) (Mishra et al., 2016) or possibly of the Tista megafan (Fig. 10A). These great earthquakes induce a millennium scale shortening rate ($13^{+7/-5}$ mm·yr^{-1}) that is one order of magnitude faster than the long time scale shortening rate (0.35-2.5 mm·yr^{-1}) of the embryonic thrust belt, suggesting that they are related to a forward propagation of the MFT, which is frequently affected by great earthquakes (Fig. 16B).

Therefore, we suggest that the embryonic fold and thrust belt has been slowly deforming for millions of years, resulting in a deformation rate one order of magnitude lower than that of the Himalayan thrust belt. Its incorporation into the Himalayan belt occurs when the frontal thrust propagates forward, cuts, or reactivates previous structures and slips during large earthquakes.

7. Conclusion

A compilation of 61 geomorphological studies indicates that the piedmont ahead of the active frontal structure of the Himalayan thrust belt is affected by deformation inducing uplift, creating relief, disturbing the drainage pattern, and locally inducing a strong incision. This deformation is evidenced from the western end to the eastern end of the Himalayas and is related to an embryonic thrust belt south of the Himalayan morphological front.

Blind thrusts and folds were imaged using several seismic profiles from the foreland basin. In the Birgunj area, the 10,000 year-scale and the 1,000,000 year-scale shortening rates, deduced from the incision and from the sediment/structure relationships, respectively, are 1 ± 0.4 mm·yr^{-1} and 2.6 ± 1.2 mm·yr^{-1}, respectively. In the Darjeeling area, blind thrusts and folds were evidenced by passive seismic records located south of the MFT. They deform the buried

Siwalik sediments below the Gish fan and the apex of the Tista megafan at a 1.1 ± 0.7 mm·yr^{-1} million year-scale shortening rate. Therefore, the shortening of the embryonic thrust belt is less than 20% and probably less than 10% of the Himalayan shortening.

In the Darjeeling area, two scarps of approximately 10 m affect the Tista megafan and are related to a 9.7 ± 5 mm·yr^{-1} 1,000 year-scale shortening rate. The frontal scarp of the Matiali Fan deforms the fan with a 7.3 ± 5 mm·yr^{-1} 1,000 year-scale shortening rate, whereas several metre-scale slip events related to earthquakes of magnitude greater than eight were detected at the base of the MFT2 scarp. The Matiali fan is also affected by two other scarps (MBT and MFT1) active since at least 60 ka, and the 10,000 year-scale shortening rate through the entire Matiali fan is 4.2 ± 2.3 mm·yr^{-1}. The recent increase in the shortening rate in the piedmont of Darjeeling is likely related to the recent propagation of seismic ruptures through the previously slowly deformed embryonic thrust belt in the piedmont of the Himalayas.

The deformation of the piedmont is spatially too limited, and its rate is too small to significantly reduce the seismic hazard linked to extremely large or large earthquakes affecting the MHT, even in a seismic gap such as that in west-central Nepal. Nonetheless, the energy absorbed during the deformation of the embryonic thrust belt was not negligible. If the elastic component is released during earthquakes, such events would be significantly damaging in the densely populated piedmont because their epicentres would be at shallow depths beneath the piedmont. Therefore, it is of utmost importance to image and precisely characterise blind structures to obtain better estimations of seismic hazards in the plain.

The different types of structures described and analysed herein provide a conceptual framework for interpreting the tectonics of the piedmont and Himalayan front and are based on A) the development of the sharp Himalayan morphological front above the emergence of great seismic ruptures along the MFT and B) the lateral and/or frontal propagation in the piedmont of seismic cycle-related deformation (these seismic rupture-related scarps are superposed to previous structures). C) The latter structures are expressed at the surface by bulges or tilts of

the topography that develop at a slow geological rate and (D) basement tectonics occur beneath the foreland basin.

The embryonic thrust belt south of the Himalayas may have remained poorly observed because of its hidden location beneath the plain. New developments in geophysics or geodetic studies, such as satellite image interferometry or precise DEM construction, will provide new data and will allow a better understanding of the present-day Himalayan deformation. It would be worthwhile to pursue interdisciplinary studies across a wide area to better determine the mechanism of long-term deformation in this setting.

Acknowledgements

We thank A. De Leeuw and J.F. Buoncristiani for numerous discussions. We thank Dr. P. Prokop and Dr. C. Goswami for sharing personal field observations and Dr. Sandip More and Dr. B. R. Gyawali for field assistance. R. Butler, R. Bilham, and F. Balsamo critically reviewed the manuscript and offered several helpful suggestions, which have led to numerous improvements. We thank them both. This work was funded in 2019 by an internal grant from the Institut des Sciences de la Terre (Grenoble) and CNRS Himal-Fan ANR-17-CE01-0018. The maps were developed using a free geographic information system (www.qgis.org).

Declaration of Competing Interest

We declare that we do not have any conflicts of interest.

Author contributions

J-L. M. performed the regional synthesis. E. L. performed the morphological analysis during his master's thesis. P.H. led the project and acquired the horizontal-to-vertical spectral ratio data that she processed with the help of E.L. and B.G.. F. J. processed the dislocation models based on GNSS data. T. C. and P. H. completed the structural synthesis in the Darjeeling area. All the authors have discussed and contributed to the writing of the manuscript. J-L.M., P.H., and E.L. drafted and finalised the manuscript.

Data Availability

Appendix A: Interactive Map Data (a *.kmz file). Yellow pines for the location of the studies compiled in Table 2; red pines for the location of the dating compiled in Fig. 10 data (Appendix B).

Appendix B: Supplementary data: Dating in the Darjeeling Piedmont (Fig. 10).

Appendix C: Supplementary data: Propagation of uncertainties related to the balancing procedures.

Appendix D: Supplementary data: Calculation of the depth of the décollement beneath the Matiali fan using balancing procedures.

REFERENCES:

Abrahami, R., Huyghe, P., Van der Beek, P., Lowick, S., Carcaillet, J., Chakraborty, T., 2018. Late Pleistocene – Holocene development of the Tista megafan (West Bengal, India): 10Be cosmogenic and IRSL age constraints. Quat. Sci. Rev. 185, 69–90. doi: 10.1016/j.quascirev.2018.02.001

Acharyya, S.K., Bhatt, D.K., Sen, M.K., 1987. Earliest Miocene planktonic foraminifera from Kalijhora area, Tista river section, Darjeeling Sub-Himalaya. Indian Minerals 41, 31–37.

Ader, T., Avouac, J.-P., Liu-Zeng, J., Lyon-Caen, H., Bollinger, L., Galetzka, J., Genrich, J., Thomas, M., Chanard, K., Sapkota, S.N., Rajaure, S., Shrestha, P., Ding, L., Flouzat, M., 2012. Convergence rate across the Nepal Himalaya and interseismic coupling on the Main Himalayan Thrust: Implications for seismic hazard. J. Geophys. Res. 117, B04403. doi: 10.1029/2011JB009071

Adilakshmi, L., Manglik, A., Thiagarajan, S. and Suresh, M., 2021. Crustal structure of the Indian plate underneath the alluvial plains of the central Ganga basin by broadband magnetotellurics. Tectonophysics, v.802, 228746.

Almeida, R.V., Hubbard, J., Liberty, L., Foster, A., Sapkota, S.N., 2018. Seismic imaging of the Main Frontal Thrust in Nepal reveals a shallow décollement and blind thrusting. Earth Planet. Sci. Lett. 494, 216–225. doi: 10.1016/j.epsl.2018.04.045

ASTER, 2011. The Advanced Spaceborne Thermal Emission and Reflection Radiometer (ASTER) Global Digital Elevation Model 30m resolution, NASA Earth Observation, https://terra.nasa.gov/about/terra-instruments/aster

Avouac, J.-P., Bollinger, L., Lavé, J., Cattin, R., Flouzat, M., 2001. Le cycle sismique en Himalaya. Comptes Rendus de l'Académie des Sciences – Series IIA – Earth Planet. Sci. 333, 513–529. doi: 10.1016/S1251-8050(01)01573-7

Avouac, J.-P., Meng, L., Wei, S., Wang, T., Ampuero, J.-P., 2015. Lower edge of locked Main Himalayan Thrust unzipped by the 2015 Gorkha earthquake. Nat. Geosci. 8, 708–711. doi: 10.1038/ngeo2518

Barrier, L., Nalpas, T., Gapais, D., Proust, J.-N., 2013. Impact of synkinematic sedimentation on the geometry and dynamics of compressive growth structures: Insights from analogue modelling. Tectonophysics 608, 737–752. doi: 10.1016/j.tecto.2013.08.005

Bashyal, R.P., 1998. Petroleum exploration in Nepal. Journal of Nepal Geological Society 19–24.

Berger, A., Jouanne, F., Hassani, R., Mugnier, J.L., 2004. Modelling the spatial distribution of present-day deformation in Nepal: how cylindrical is the Main Himalayan Thrust in Nepal? Geophys. J. Int. 156, 94–114. doi: 10.1111/j.1365-246X.2004.02038.x

Bhattacharya, A., Arora, M. K., Sharma, M. L., Vöge, M., Bhasin, R., 2014. Surface displacement estimation using space-borne SAR interferometry in a small portion along Himalayan Frontal Fault. Opt. Lasers Eng., 53, 164–178. doi: 10.1016/j.optlaseng.2013.09.001

Bilham, R., 2019. Himalayan earthquakes: a review of historical seismicity and early 21st century slip potential. Geol. Soc. Lon. Spec. Publ. 483, 423–482. doi: 10.1144/SP483.16

Bilham, R., Mencin D., Bendick R., Bürgmann R., 2017. Implications for elastic energy storage in the Himalaya from the Gorkha 2015 earthquake and other incomplete ruptures of the Main Himalayan Thrust. Quaternary International 462, 3-21. doi:10.1016/j.quaint.2016.09.055

1250 Bilham, R., Gaur, V.K., Molnar, P., 2001. Himalayan Seismic Hazard. Science 293, 1442-1444.
1251 doi: 10.1126/science.1062584
1252 Bilham, R., Blume, F. Bendick, R., Gaur,V., 1998. Geodetic constraints on the translation and
1253 deformation of India: Implications for future great Himalayan earthquakes. Current
1254 Science, 74, 213-229.
1255 Bilham, R., Larson, K., Freymueller, J. and IDYLHIM team, 1997. GPS measurements of
1256 present-day convergence across the Nepal Himalaya. Nature 386, 61–64. doi:
1257 10.1038/386061a0
1258 Bollinger, L., Sapkota, S.N., Tapponnier, P., Klinger, Y., Rizza, M., Van der Woerd, J., Tiwari,
1259 D.R., Pandey, R., Bitri, A., Bes de Berc, S., 2014. Estimating the return times of great
1260 Himalayan earthquakes in eastern Nepal: Evidence from the Patu and Bardibas
1261 strands of the Main Frontal Thrust: Return period of Himalayan earthquakes. J.
1262 Geophys. Res. Solid Earth 119, 7123–7163. doi: 10.1002/2014JB010970
1263 Bonnet, C., Malavieille, J., Mosar, J., 2008. Surface processes versus kinematics of thrust
1264 belts: impact on rates of erosion, sedimentation, and exhumation – Insights from
1265 analogue models. Bull. Soc. Géol. Fr. 179, 297–314. doi: 10.2113/gssgfbull.179.3.297
1266 Boyer, S. E., Elliott, D. 1982. The geometry of thrust systems. Bull. Am. Ass. Petrol. Geol. 66,
1267 1196-1230.
1268 Burbank, D.W., and Anderson, R.S., 2011. Tectonic Geomorphology; 2nd edition: Wiley, 454
1269 pp. doi: 10.14241/asgp.2017.016
1270 Burgess, W.P., Yin, A., Dubey, C.S., Shen, Z.-K., Kelty, T.K., 2012. Holocene shortening across
1271 the Main Frontal Thrust zone in the eastern Himalaya. Earth Planet. Sci. Lett. 357–
1272 358, 152–167. doi: 10.1016/j.epsl.2012.09.040
1273 Butler, R.W.H., 1982. The terminology of structures in thrust belts. Journal of Structural
1274 Geology, 4, 239-245.
1275 Butler, R.W.H., 2020. Syn-kinematic strata influence the structural evolution of emergent
1276 fold–thrust belts. Geol. Soc. Lon. Spec. Publ. 490, 57–78. doi: 10.1144/SP490-2019-14
1277 Chakraborty, T., Ghosh, P., 2010. The geomorphology and sedimentology of the Tista
1278 megafan, Darjeeling Himalaya: implications for megafan building processes.
1279 Geomorphology 115, 252-266. doi: 10.1016/j.geomorph.2009.06.035
1280 Chakraborti, T., Taral, S., More, S., Bera, S., 2020. Cenozoic Himalayan Foreland Basin: An
1281 Overview and Regional Perspective of the Evolving Sedimentary Succession. In
1282 Springler Geology, Geodynamics of the Indian Plate, N. Gupta, S. K. Tandon (eds.)p.
1283 395-437. doi: 10.1007/978-3-030-15989-4_11
1284 Chalaron, E., Mugnier, J.L., Mascle, G., 1995. Control on thrust tectonics in the Himalayan
1285 foothills: a view from a numerical model. Tectonophysics 248, 139–163. doi:
1286 10.1016/0040-1951(94)00281-D
1287 Chamberlin, R.T., 1910. The Appalachian folds of central Pennsylvania. Journal of Geology 18,
1288 228-251.
1289 Champel, B., Van der Beek, P., Mugnier, J.-L., Leturmy, P., 2002. Growth and lateral
1290 propagation of fault-related folds in the Siwaliks of western Nepal: Rates,
1291 mechanisms, and geomorphic signature. J. Geophys. Res. 107, 2111. doi:
1292 10.1029/2001JB000578
1293 Chandra, U., 1992. Seismotectonics of Himalaya. Current Science (Bungalore) 62, 40–71
1294 Chirouze, F., Huyghe, P., Van der Beek, P., Chauvel, C., Chakraborty, T., Dupont-Nivet, G.,
1295 Bernet, M., 2013. Tectonics, exhumation, and drainage evolution of the eastern
1296 Himalaya since 13 Ma from detrital geochemistry and thermochronology, Kameng

River Section, Arunachal Pradesh. Geol. Soc. Am. Bull. 125, 523–538. doi: 10.1130/B30697.1

Cook, K., Turowski, J., Hovius, N., 2012. A natural experiment demonstrating the importance of bedload transport for fluvial bedrock erosion and knickpoint propagation. AGU Fall Meeting Abstracts, pp. EP44A-08.

Cortés-Aranda, J., Mugnier, J.-L., Jouanne, F., Vassallo, R., Carcaillet, J., Alam Awan, A., 2017. Holocene shortening rates and seismic hazard assessment for the frontal Potwar Plateau, NW Himalaya of Pakistan: Insights from 10 Be concentrations on fluvial terraces of the Mahesian Anticline. Quat. Int. 462, 75–89. doi: 10.1016/j.quaint.2017.02.032

Coutand, I., Barrier, L., Govin, G., Grujic, D., Hoorn, C., Dupont-Nivet, G., Najman, Y. , 2016. Late Miocene-Pleistocene evolution of India-Eurasia convergence partitioning between the Bhutan Himalaya and the Shillong Plateau: new evidences from foreland basin deposits along the Dungsam Chu section, eastern Bhutan. Tectonics 35, 2963–2994. doi: 10.1002/2016TC004258

Dahlstrom, C. D., 1970. Structural geology in the eastern margin of Canadian Rocky Mountains. Bull. Can. Petrol. Geol. 18, 332-406.

Dal Zilio, L., Jolivet, R., van Dinther, Y., 2020. Segmentation of the Main Himalayan Thrust illuminated by Bayesian inference of interseismic coupling. Geophysical Research Letters, 47, e2019GL086424. https://doi.org/10.1029/2019GL086424

Dal Zilio, L., Van Dinther, Y., Gerya, T., Avouac, J.-P., 2019. Bimodal seismicity in the Himalaya controlled by fault friction and geometry. Nat. Commun. 10, 48. doi: 10.1038/s41467-018-07874-8

Das, A., Chattopadhyay, G.S., 1993. Neotectonics in the Tista, Jaldhaka and Torsa Interfluve belt of North Bengal. Geol. Surv. India Rec. 121, 101–109.

Dasgupta, S., Mazumdar, K., Moirangcha, L.H., Gupta, T.D., Mukhopadhyay, B., 2013. Seismic landscape from Sarpang re-entrant, Bhutan Himalaya foredeep, Assam, India: Constraints from geomorphology and geology. Tectonophysics 592, 130–140. doi: 10.1016/j.tecto.2013.02.021

DeCelles, P.G., Carrapa, B., 2021. Coupled Rapid Erosion and Foreland Sedimentation Control Orogenic Wedge Kinematics in the Himalayan Thrust Belt of Central Nepal. J. Geophys. Res. Solid Earth. doi: 10.1029/2020JB021256

DeCelles, P.G., Gehrels, G.E., Quade, J., Ojha, T.P., 1998. Eocene-early Miocene foreland basin development and the history of Himalayan thrusting, western and central Nepal. Tectonics 17, 741–765. doi: 10.1029/98TC02598

Delcaillau, B., 1986. Dynamique et évolution morphostructurale du piémont frontal de l'Himalaya: les Siwaliks du Népal oriental. Revue de géologie dynamique et de géographie physique 27, 319–337.

Delcaillau, B., Carozza, J.-M., Laville, E., 2006. Recent fold growth and drainage development: The Janauri and Chandigarh anticlines in the Siwalik foothills, northwest India. Geomorphology 76, 241–256. doi: 10.1016/j.geomorph.2005.11.005

Dey, S., Thiede, R.C., Schildgen, T.F., Wittmann, H., Bookhagen, B., Scherler, D., Jain, V., Strecker, M.R., 2016. Climate-driven sediment aggradation and incision since the late Pleistocene in the NW Himalaya, India. Earth Planet. Sci. Lett. 449, 321–331. doi: 10.1016/j.epsl.2016.05.050

Dhital, M.R., 2015. Geology of the Nepal Himalaya, Regional Geology Reviews. Springer International Publishing, Cham. doi: 10.1007/978-3-319-02496-7

1344 Divyadarshini, A., Tandon,S., 2022. Transverse tectonic features of the Himalaya and sub-
1345 surface basement structures of the foreland basin: implications for orogenic
1346 segmentation and seismicity distribution. Himalayan Geology, 43, 180-200.
1347 Divyadarshini, A., Singh, V., 2019. Investigating topographic metrics to decipher structural
1348 model and morphotectonic evolution of the Frontal Siwalik Ranges, Central Himalaya,
1349 Nepal. Geomorphology 337, 31–52. doi: 10.1016/j.geomorph.2019.03.028
1350 Divyadarshini, A., Singh, V., Jaiswal, M.K., Rawat, M., 2020. Exploring the roles of climate and
1351 tectonics in the geomorphic evolution of the Chitwan Intermontane valley, Central
1352 Himalaya. Geomorphology 367, 107298. doi: 10.1016/j.geomorph.2020.107298.
1353 DMG, 1990. Exploration opportunities in Nepal. Executive summary of the seminar organized
1354 by Department of Mines and Geology (Nepal), London, 8 march 1990. 32 pages.
1355 Dunn, J., Auden, J., Roy, S., 1939. The Bihar–Nepal Earthquake of 1934. Mem. Geol. Soc. of
1356 India, 73. Survey of India, Calcuta (391 pp.).
1357 Duroy, Y., Farah, A., Lillie, R., 1989. Subsurface densities and lithospheric flexure of the
1358 Himalayan foreland in Pakistan. In "Tectonics of the western Himalayas" edited by
1359 Lawrence L. Malinconico, Jr. and Robert J. Lillie. GSA special paper 232, 217-233. doi:
1360 10.1130/SPE232-p217
1361 Duvall M.,Waldron J.,Godin L., Najman Y., 2020. Active strike-slip faults and an outer frontal
1362 thrust in the Himalayan foreland basin. PNAS 117, 17615-17621. doi:
1363 10.1073/pnas.2001979117
1364 Elliott, J.R., Jolivet, R., González, P.J., Avouac, J.-P., Hollingsworth, J., Searle, M.P., Stevens,
1365 V.L., 2016. Himalayan megathrust geometry and relation to topography revealed by
1366 the Gorkha earthquake. Nat. Geosci. 9, 174–180. doi: 10.1038/ngeo2623
1367 Epard, J.-L., Groshong, R.H., Jr., 1993. Excess Area and Depth to Detachment. AAPG Bull. 77,
1368 1291–1302. doi: 10.1306/BDFF8E66-1718-11D7-8645000102C1865D
1369 Fagereng, Å., Biggs, J., 2019. New perspectives on 'geological strain rates' calculated from
1370 both naturally deformed and actively deforming rocks. J. Struct. Geol. 125, 100–110.
1371 doi: 10.1016/j.jsg.2018.10.004
1372 Flouzat, M., Bettinelli, P., Willis, P., Avouac, J.-P., Héritier, T., Gautam, U., 2009. Investigating
1373 tropospheric effects and seasonal position variations in GPS and DORIS time-series
1374 from the Nepal Himalaya. Geophys. J. Int. 178, 1246–1259. doi: 10.1111/j.1365-
1375 246X.2009.04252.x
1376 Friedenreich, O.R., Slind, O.L., Pradhan, U.M.S., Shresta, R.B., 1994. Petroleum Geology of
1377 Nepal. Canadian J. Exploration Geophys. 30, 103–114.
1378 Gansser, A., 1964. Geology of the Himalayas. Reg. Geol. Series. Ed. L. U. de Sitter
1379 Gansser, A., 1983. Geology of the Bhutan Himalaya. 181 pp. Geol. Magazine, 121(2), 133-134.
1380 doi: 10.1017/S0016756800028120
1381 Gautam, P., Rösler, W., 1999. Depositional chronology and fabric of Siwalik group sediments
1382 in Central Nepal from magnetostratigraphy and magnetic anisotropy. J. Asian Earth
1383 Sci. 17, 659–682. doi: 10.1016/S1367-9120(99)00021-8
1384 Gibling, M.R., Tandon, S.K., Sinha, R., Jain, M., 2005. Discontinuity bounded alluvial
1385 sequences of the southern gangetic plains, India: Aggradation and degradation in
1386 response to monsoonal strength. J. Sediment. Res. 75, 369–385. doi:
1387 10.2110/jsr.2005.029
1388 Godin, L., Harris, L.B., 2014. Tracking basement cross-strike discontinuities in the Indian crust
1389 beneath the Himalayan orogen using gravity data – relationship to upper crustal
1390 faults. Geophys. J. Int. 198, 198–215. doi: 10.1093/gji/ggu131

1391 Godin, L., Soucy La Roche, R., Waffle, L., Harris, L.B., 2019. Influence of inherited Indian
1392 basement faults on the evolution of the Himalayan Orogen. Geol. Soc. Lon. Spec.
1393 Publ. 481, 251–276. doi: 10.1144/SP481.4

1394 Goguel, J., 1952. Traité de tectonique. Revue de Géographie Alpine. 41-3, 595-597.

1395 Gonzalez-Mieres, R., Suppe, J., 2006. Relief and shortening in detachment folds. J. Struct.
1396 Geol. 28, 1785–1807. doi: 10.1016/j.jsg.2006.07.001

1397 Gonzalez-Mieres, R., Suppe, J., 2011. Shortening histories in active detachment folds based
1398 on area-of-relief methods. Thrust Fault-related Folding: AAPG Memoir 94. 39-67 doi:
1399 10.1306/13251332M943428

1400 Goswami, C., 2012. Geomorphic evidences of active faulting in the northwestern Ganga
1401 Plain, India: implications for the impact of basement structures. Geosciences Journal
1402 16, 289 – 299.

1403 Goswami, C., Mukhopadhyay, D., Poddar, B.C., 2012. Tectonic control on the drainage system
1404 in a piedmont region in tectonically active eastern Himalayas. Front. Earth Sci. 6, 29–
1405 38. doi: 10.1007/s11707-012-0297-z

1406 Goswami, C. C., Mukhopadhyay, D., Poddar, B.C., 2013. Geomorphology in relation to
1407 tectonics: A case study from the eastern Himalayan foothills of West Bengal, India.
1408 Quat. Int. 298, 80–92. doi: 10.1016/j.quaint.2012.12.020

1409 Goswami, C., Jana, P., Weber, J.C., 2019. Evolution of landscape in a piedmont section of
1410 Eastern Himalayan foothills along India-Bhutan border: A tectono-geomorphic
1411 perspective. Journal of Mountain Sci. 16, 2828–2843.
1412 https://doi.org/10.1007/s11629-018-5208-7

1413 Grandin, R., Vallée, M., Satriano, C., Lacassin, R., Klinger, Y., Simoes, M., Bollinger, L., 2015.
1414 Rupture process of the M_w = 7.9 2015 Gorkha earthquake (Nepal): Insights into
1415 Himalayan megathrust segmentation. Geophys. Res. Lett. 42, 8373–8382. doi:
1416 10.1002/2015GL066044

1417 Gratier, J.-P., Gueydan F., 2007. Deformation in the presence of fluids and minerals: Effect of
1418 fracturing andfluid-rock interaction onseismic cycles, in Tectonic Faults: Agents of
1419 Change on a Dynamic Earth, 95, edited by M. R. Handy, G. Hirth, and N. Hovius, pp.
1420 319–356, Dahlem Univ. Press., London, U. K

1421 Grimaud, J.-L., Paola, C., Ellis, C., 2017. Competition between uplift and transverse
1422 sedimentation in an experimental delta: Uplift Versus Transverse Sedimentation. J.
1423 Geophys. Res. Earth Surf. 122, 1339–1354. doi: 10.1002/2017JF004239

1424 Guéguen, P., Cornou, C., Garambois, S., Banton, J., 2007. On the Limitation of the H/V
1425 Spectral Ratio Using Seismic Noise as an Exploration Tool: Application to the Grenoble
1426 Valley (France), a Small Apex Ratio Basin. Pure appl. Geophys. 164, 115–134. doi:
1427 10.1007/s00024-006-0151-x

1428 Guha, D., Bardhan, S., Basir, S., De, A., Sarkar, A., 2007. Imprints of Himalayan thrust tectonics
1429 on the quaternary piedmont sediments of the Neora-Jaldhaka valley, Darjeeling-
1430 Sikkim sub-Himalayas, India. J. Asian Earth Sci. 30, 464–473. doi:
1431 10.1016/j.jseaes.2006.11.010

1432 Gupta, T.D., Mukhopadhyay, B., Dasgupta S., Roy, S., 2017. Neo-tectonic activity in Sarpang
1433 Re-entrant, frontal Bhutan Himalaya, Kokrajhar District, Assam, India: Constrain from
1434 geological, geomorphological and GPS surveys. Indian Journal of Geosciences 71, 181-
1435 194.

1436 Hack, J.T., 1973. Stream-profile analysis and stream-gradient index. J. Res. U.S. Geol. Survey 1,
1437 421–429.

1438 Harrison, T.M., Copeland, P., Hall, S.A., Quade, J., Burner, S., Ojha, T.P., Kidd, W.S.F., 1993.
1439 Isotopic Preservation of Himalayan/Tibetan Uplift, Denudation, and Climatic Histories
1440 of Two Molasse Deposits. J. Geol. 101, 157–175. doi: 10.1086/648214
1441 Hartley, A., Weismann G., Bhattacharayya, P., Nichols, G., Scuderi, L., Davidson, S.,Leleu, S.,
1442 Chakraborty, T., Ghosh, P., 2013. Soil development on modern distributive fluvial
1443 system: preliminary observations with interpretation of paleosols in the rock record.
1444 In: New Frontiers in Paleopedology and Terrestrial Paleoclimatology, p. 149–158. DOI:
1445 10.2110/sepmsp.104.10
1446 Hinzen, K.-G., Weber, B., Scherbaum, F., 2004. On the resolution of H/V measurements to
1447 determine sediment thickness, a case study across a normal fault in the Lower Rhine
1448 Embayment, Germany. J. Earth. Eng. 08, 909–926. doi: 10.1142/S136324690400178X
1449 Hodges, K.V., Wobus, C., Ruhl, K., Schildgen, T., Whipple, K., 2004. Quaternary deformation,
1450 river steepening, and heavy precipitation at the front of the Higher Himalayan ranges.
1451 Earth Planet. Sci. Lett. 220, 379–389. doi: 10.1016/S0012-821X(04)00063-9
1452 Husson L., Mugnier J.L., 2003. Three dimensional Horizon Reconstruction from Outcrop
1453 Structural Data, Restoration and Strain Fields of the Baisahi anticline, Western Nepal,
1454 Journal of Structural Geology 25, 79-90.
1455 Jackson, M., Bilham, R., 1994. Constraints on Himalayan deformation inferred from vertical
1456 velocity fields in Nepal and Tibet. J. Geophys. Res. 99, 13897–13912. doi:
1457 10.1029/94JB00714
1458 Jain, V., Sinha, R., 2003. River systems in the Gangetic plains and their comparison with the
1459 Siwaliks: a review. Current Science 84, 1025-1033
1460 Jain, V., Sinha, R., 2005. Response of active tectonics on the alluvial Baghmati River,
1461 Himalayan foreland basin, eastern India. Geomorphology 70, 339–356. doi:
1462 10.1016/j.geomorph.2005.02.012
1463 Jayangondaperumal, R., Mugnier, J.L., Dubey, A. K., 2013. Earthquake slip estimation from
1464 the scarp geometry of Himalayan Frontal Thrust, western Himalaya: Implications for
1465 seismic hazard assessment, Int. J. Earth Sci. 102, 1937–1955. doi: 10.1007/s00531-
1466 013-0888-2
1467 Jayangondaperumal, R., Wesnousky, S.G., Choudhuri, B.K., 2011. Near-Surface Expression of
1468 Early to Late Holocene Displacement along the Northeastern Himalayan Frontal
1469 Thrust at Marbang Korong Creek, Arunachal Pradesh, India. Bull. Seismol. Soc. Am.
1470 101, 3060–3064. doi: 10.1785/0120110051
1471 Jolivet, R., Frank, W.B., 2020. The Transient and Intermittent Nature of Slow Slip. AGU
1472 Advances 1. doi: 10.1029/2019AV000126
1473 Jouanne, F., Gajurel, A., Mugnier, J.-L., Bollinger, L., Adhikari, L.B., Koirala, B., Cotte, N.,
1474 Bhattarai, R., Pecher, A., Bascou, P., Huyghe, P., 2019. Postseismic deformation
1475 following the April 25, 2015 Gorkha earthquake (Nepal): Afterslip versus viscous
1476 relaxation. J. Asian Earth Sci. 176, 105–119. doi: 10.1016/j.jseaes.2019.02.009
1477 Jouanne, F., Mugnier, J.L., Sapkota, S.N., Bascou, P., Pecher, A., 2017. Estimation of coupling
1478 along the Main Himalayan Thrust in the central Himalaya. J. Asian Earth Sci. 133, 62–
1479 71. doi: 10.1016/j.jseaes.2016.05.028
1480 Kaneda, H., Nakata, T., Tsutsumi, H., Kondo, H., Sugito, N., Awata, Y., Akhtar, S.S., Majid, A.,
1481 Khattak, W., Awan, A.A., Yeats, R.S., Hussain, A., Ashraf, M., Wesnousky, S.G., Kausar,
1482 A.B., 2008. Surface Rupture of the 2005 Kashmir, Pakistan, Earthquake and Its Active
1483 Tectonic Implications. Bull. Seismol. Soc. Am. 98, 521–557. doi: 10.1785/0120070073

Kar, R., Chakraborty, T., 2014. Comment on “Geomorphology in relation to tectonics: a case study from the eastern Himalayan foothill of West Bengal, India” by Chandreyee Goswami, Dhruba Mukhopadhyay, B. C. Poddar. Quat. Int. 338, 113-118. doi: 10.1016/j.quaint.2014.01.041

Kar, R., Chakraborty, T., Chakraborty, C., Ghosh, P., Tyagi, A.K., Singhvi, A.K., 2014. Morpho-sedimentary characteristics of the Quaternary Matiali fan and associated river terraces, Jalpaiguri, India: Implications for climatic controls. Geomorphology 227, 137–152. doi: 10.1016/j.geomorph.2014.05.014

Karunakaran, C., Rao, A.R., 1976. Status of exploration for hydrocarbons in the Himalayan region—contributions to stratigraphy and structure. Geol. Surv. India Misc. Publ. 41 (5), 1–66.

Keller, E.A., Pinter, N., 2002. Active Tectonics: Earthquakes, uplift, and landscape. 2nd Edition, Prentice Hall, Upper Saddle River, 362p.

Kralia, A., Thakur, M., 2021. Geomorphic mapping and investigation of the uplifted piedmont zone between Haridwar and Kotdwar, Indo-Gangetic Plain, India. App. Comput. Geosci. 9, 100047. doi: 10.1016/j.acags.2020.100047

Kumahara, Y., Jayangondaperumal, R., 2013. Paleoseismic evidence of a surface rupture along the northwestern HimalayanFrontal Thrust (HFT). Geomorphology 180-181, 47-56. doi: 10.1016/j.geomorph.2012.09.004

Kumar, S., Wesnousky, S.G., Jayangondaperumal, R., Nakata, T., Kumahara, Y., Singh, V., 2010. Paleoseismological evidence of surface faulting along the northeastern Himalayan front, India: Timing, size, and spatial extent of great earthquakes. J. Geophys. Res. 115, B12422. doi: 10.1029/2009JB006789

Kumar, S., Wesnousky, S.G., Rockwell, T.K., Briggs, R.W., Thakur, V.C., Jayangondaperumal, R., 2006. Paleoseismic evidence of great surface rupture earthquakes along the Indian Himalaya. J. Geophys. Res. 111, B03304. doi: 10.1029/2004JB003309

Kumar, S., Wesnousky, S.G., Rockwell, T.K., Ragona, D., Thakur, V.C., Seitz, G.G., 2001. Earthquake Recurrence and Rupture Dynamics of Himalayan Frontal Thrust, India. Science 294, 2328–2331. doi: 10.1126/science.1066195

Large, E., Huyghe, P., Mugnier, J-L., Guillier, B., Taral, S., Gyawali, B.R., Chabraborty, T., accepted. Distribution of active tectonics in the Himalayan piedmont (Darjeeling, Eastern India) inferred from Horizontal-to-Vertical Spectral Ratio analysis of passive seismic records. Terra Nova. https://www.isterre.fr/annuaire/pages-web-du-personnel/jean-louis-mugnier/document-de-travail/article/manuscript-terra-nova.html?var_mode=calcul

Lavé, J., Avouac, J.P., 2000. Active folding of fluvial terraces across the Siwaliks Hills, Himalayas of central Nepal. J. Geophys. Res. 105, 5735–5770. doi: 10.1029/1999JB900292

Lavé, J., Yule, D., Sapkota, S., Basant, K., Madden, C., Attal, M., Pandey, R., 2005. Evidence for a Great Medieval Earthquake (1100 A.D.) in the Central Himalayas, Nepal. Science 307, 1302–1305. doi: 10.1126/science.1104804

Le Béon, M., Marc, O., Suppe, J., Huang, M., Huang, S., Chen, W., 2019. Structure and Deformation History of the Rapidly Growing Tainan Anticline at the Deformation Front of the Taiwan Mountain Belt. Tectonics 38, 3311–3334. doi: 10.1029/2019TC005510

Le Fort, P., 1975. Himalayas: the collided range. Present knowledge of the continental arc. Am. J. Sci. 275, 1–44.

Le Roux-Mallouf, R., Ferry, M., Cattin, R., Ritz, J.-F., Drukpa, D., Pelgay, P., 2020. A 2600-year-long paleoseismic record for the Himalayan Main Frontal Thrust (western Bhutan). Solid Earth 11, 2359–2375. doi: 10.5194/se-11-2359-2020

Le Roux-Mallouf, R., Ferry, M., Ritz, J.-F., Berthet, T., Cattin, R., Drukpa, D., 2016. First paleoseismic evidence for great surface-rupturing earthquakes in the Bhutan Himalayas. J. Geophys. Res.: Solid Earth 121, 7271–7283.doi : 10.1002/2015JB012733

Leturmy, P., 1997. Sédiments et reliefs du front des systèmes chevauchants : modélisation et exemples du front andin et des Siwalik (Himalaya) à l'Holocène (Tectonique). Université Joseph Fourier, Grenoble 1. 236 p.

Makaske, B., 2001. Anastomosing rivers: a review of their classification, origin and sedimentary products. Earth Sci. Rev. 53, 149–196. doi: 10.1016/S0012-8252(00)00038-6

Malik J.N., Sahoo A.K., Shah A.A., Shinde D.P., Juyal N.,Singhvi A.K., 2010. Paleoseismic evidence from trench investigation along Hajipur Fault, Himalayan Frontal Thrust, NW Himalaya: implication of the faulting pattern on landscape evolution and seismic hazard. J. Struct. Geol. 32:350–361. doi: 10.1016/j.jsg.2010.01.005

Mallick, R., Bürgmann, R., Johnson, K., & Hubbard, J. (2021). A unified framework for earthquake sequences and the growth of geological structure in fold-thrust belts. Journal of Geophysical Research: Solid Earth, 126, e2021JB022045. https://doi.org/10.1029/2021JB022045

Manglik, A., Kandregula R.S., Pavankumar, G., 2022. Foreland Basin Geometry and Disposition of Major Thrust Faults as Proxies for Identification of Segmentation along the Himalayan Arc. Jour. Geol. Soc. India 98:57-61. https://doi.org/10.1007/s12594-022-1928-y

McDougall, J.W., Hussain, A., Yeats, R.S., 1993. The Main Boundary Thrust and propagation of deformation into the foreland fold-and-thrust belt in northern Pakistan near the Indus River. Geol. Soc. Lon. Spec. Publ. 74, 581–588. doi: 10.1144/GSL.SP.1993.074.01.38

Mencin et aL., 2016. Mencin, D., Bendick, R., Upreti, B., Adhikari, D., Gajurel, A., Bhattarai, R., Shrestha, H., Bhattarai, T., Manandhar, N., Galetzka, J., Knappe, E., Pratt-Sitaula, B., Aoudia, A., Bilham, R., 2016. Himalayan strain reservoir inferred from limited afterslip following the Gorkha earthquake. Nat. Geosci. http://dx.doi.org/10.1038/ngeo2734.

Mial, A., 2013. The geology of fluvial deposits: sedimentary facies, basin analysis, and petroleum geology. Edited by Springler, 582 pp.

Mishra, R.L., Singh, I., Pandey, A., Rao, P.S., Sahoo, H.K., Jayangondaperumal, R., 2016. Paleoseismic evidence of a giant medieval earthquake in the eastern Himalaya: Rupture Length of A.D. 1255 Earthquake. Geophys. Res. Lett. 43, 5707–5715. doi: 10.1002/2016GL068739

Misra, A., Agarwal, K.K., Kothyari, G.Ch., Talukdar, R., Joshi, G., 2020. Quantitative Geomorphic Approach for Identifying Active Deformation in the Foreland Region of Central Indo-Nepal Himalaya. Geotectonics 54, 543–562. doi: 10.1134/S0016852120040093

Mitra, G., 1994. Strain variation in thrust sheets across the Sevier fold-and-thrust belt (Idaho-Utah-Wyoming): implications for section restoration and wedge taper evolution. J. Struct. Geol. 16, 585–602. doi 10.1016/0191-8141(94)90099-X

Mitra, S., 2003. A unified kinematic model for the evolution of detachment folds, Journal of Structural Geology, 25: 1659-1673

1578 Molnar, P., 1987. Inversion of profiles of uplift rates for the geometry of dip-slip faults at
1579 depth, with examples from the Alps and the Himalaya. Presented at the Annales
1580 geophysicae. Series B. Terrestrial and Planet. Phys., pp. 663–670.
1581 Moretti,I., Callot, J.P., 2012. Area, length and thickness conservation: Dogma or reality?.
1582 Journal of Structural Geology, 41, 64-75.
1583 Mugnier, J. L., Baby, P., Coletta, B., Vinour, P., Bale, P., Leturmy, P., 1997. Thrust geometry
1584 controlled by erosion and sedimentation: a view from analogue models. Geology 25,
1585 427-430. doi: 10.1130/0091-7613(1997)025<0427:TGCBEA>2.3.CO;2
1586 Mugnier, J.-L., Delcaillau, B., Huyghe, P., Leturmy, P., 1998. The break-back thrust splay of the
1587 Main Dun Thrust (Himalayas of western Nepal): evidence of an intermediate
1588 displacement scale between earthquake slip and finite geometry of thrust systems. J.
1589 Struct. Geol. 20, 857–864. doi: 10.1016/S0191-8141(98)00024-8
1590 Mugnier, J.-L., Gajurel, A., Huyghe, P., Jayangondaperumal, R., Jouanne, F., Upreti, B., 2013.
1591 Structural interpretation of the great earthquakes of the last millennium in the
1592 central Himalaya. Earth Sci. Rev. 127, 30–47. doi: 10.1016/j.earscirev.2013.09.003
1593 Mugnier, J.-L., Huyghe, P., 2006. Ganges basin geometry records a pre-15 Ma isostatic
1594 rebound of Himalaya. Geology 34, 445. doi: 10.1130/G22089.1
1595 Mugnier, J.-L., Huyghe, P., Gajurel, A.P., Becel, D., 2005. Frontal and piggy-back seismic
1596 ruptures in the external thrust belt of Western Nepal. J. Asian Earth Sci. 707–717. doi:
1597 *10.1016/j.jseaes.2004.05.009*
1598 Mugnier, J.-L., Huyghe, P., Leturmy, P., Jouanne, F., 2004. Episodicity and Rates of Thrust-sheet
1599 Motion in the Himalayas (Western Nepal). Thrust tectonics and hydrocarbon systems:
1600 AAPG Memoir 82, 91–114.
1601 Mugnier, J.-L., Jouanne, F., Bhattarai, R., Cortes-Aranda, J., Gajurel, A., Leturmy, P., Robert, X.,
1602 Upreti, B., Vassallo, R., 2017. Segmentation of the Himalayan megathrust around the
1603 Gorkha earthquake (25 April 2015) in Nepal. J. Asian Earth Sci. 141, 236–252. doi:
1604 10.1016/j.jseaes.2017.01.015
1605 Mugnier, J.L., Leturmy, P., Mascle, G., Huyghe, P., Chalaron, E., Vidal, G., Husson, L., Delcaillau,
1606 B., 1999a. The Siwaliks of western Nepal. I. Geometry of the thrust wedge. J. Asian
1607 Earth Sci. 17, 629–642. doi: 10.1016/S1367-9120(99)00038-3
1608 Mugnier, J.-L., Mascle, G., Faucher, T., 1993. Structure of the Siwaliks of Western Nepal: an
1609 intracontinental accretionary prism. Int. Geol. Rev. 35, 1–16. doi:
1610 10.1080/00206819309465510
1611 Mukul, M., 2000. The geometry and kinematics of the Main Boundary Thrust and related
1612 neotectonics in the Darjiling Himalayan fold-and-thrust belt, West Bengal, India. J.
1613 Struct. Geol. 22, 1261–1283. doi: 10.1016/S0191-8141(00)00032-8
1614 Mukul, M., 2010. First-order kinematics of wedge-scale active Himalayan deformation:
1615 Insights from Darjiling–Sikkim–Tibet (DaSiT) wedge. J. Asian Earth Sci. 39, 645–657.
1616 doi: 10.1016/j.jseaes.2010.04.029
1617 Mukul, M., Jaiswal, M., Singhvi, A.K., 2007. Timing of recent out-of-sequence active
1618 deformation in the frontal Himalayan wedge: Insights from the Darjiling sub-
1619 Himalaya, India. Geology 35, 999. doi: 10.1130/G23869A.1
1620 Mullick, M., Riguzzi, F., Mukhopadhyay, D., 2009. Estimates of motion and strain rates across
1621 active faults in the frontal part of eastern Himalayas in North Bengal from GPS
1622 measurements. Terra Nova 21, 410–415.

1623 Nakamura, Y., 1989. A method for dynamic characteristics estimation of subsurface using
1624 microtremor on the ground surface. Railway Technical Research Institute, Quarterly
1625 Reports 30.
1626 Nakata, T., 1989. Active faults of the Himalaya of India and Nepal. Geol. Soc. Am. pp. 243–
1627 264. doi: 10.1130/SPE232-p243
1628 Ojha, T.P., Butler, R.F., DeCelles, P.G., Quade, J., 2009. Magnetic polarity stratigraphy of the
1629 Neogene foreland basin deposits of Nepal. Basin Res. 21, 61–90. doi: 10.1111/j.1365-
1630 2117.2008.00374.x
1631 Ori, G., Friend, P., 1994. Sedimentary basins formed and carried piggy-back on active thrust
1632 sheets. Geology. 12, 475–478. doi:10.1130/0091-7613(1984)12<475:sbfacp>2.0.co;2.
1633 Pandey, A. Jayangondaperumal, R., Hetényi, G., Priyanka, R., Singh, I., Srivastava, P.,
1634 Srivastava, H., 2021. Establishing primary surface rupture evidence and magnitude of
1635 the 1697 CE Sadiya earthquake at the Eastern Himalayan Frontal thrust, India.Nature
1636 Sci. Rep. 11, 879. doi: 10.1038/s41598-020-79571-w
1637 Pandey, M.R., Tandukar, R.P., Avouac, J.P., Vergne, J., Héritier, T., 1999. Seismotectonics of the
1638 Nepal Himalaya from a local seismic network. J. Asian Earth Sci. 17, 703–712. doi:
1639 10.1016/S1367-9120(99)00034-6
1640 Parkash, B., Kumar, S., Rao, MS., Giri, SC., Kumar, CS., Gupta, S., Srivastava, P., 2000. Holocene
1641 tectonic movements and stress field in the western Gangetic plains. Curr Sci 79:438–
1642 449
1643 Pathier, E., Fielding, E.J., Wright, T.J., Walker, R., Parsons, B.E., Hensley, S., 2006.
1644 Displacement field and slip distribution of the 2005 Kashmir earthquake from SAR
1645 imagery. Geophys. Res. Lett. 33, L20310. Doi: 10.1029/2006GL027193
1646 Pati, P., Parkash, B., Awasthi, A.K., Jakhmola, R.P., 2012. Spatial and temporal distribution of
1647 inland fans/terminal fans between the Ghaghara and Kosi rivers indicate eastward
1648 shift of neotectonic activities along the Himalayan front. A study from parts of the
1649 upper and middle Gangetic plains, India. Earth Sci. Rev. 115, 201–216. doi:
1650 10.1016/j.earscirev.2012.10.006
1651 Pati, P., Pradhan, R.M., Dash, C., Parkash, B., Awasthi, A.K., 2015. Terminal fans and the
1652 Ganga plain tectonism: A study of neotectonism and segmentation episodes of the
1653 Indo-Gangetic foreland basin, India. Earth Sci. Rev. 148, 134–149. doi:
1654 10.1016/j.earscirev.2015.06.002
1655 Patra A., Saha, D., 2019. Stress regime changes in the Main Boundary Thrust zone, Eastern
1656 Himalaya, decoded from fault setup analysis. Journal of structural geology 120, 29–
1657 42. https://doi.org/10.1016/j.jsg.2018.12.010
1658 Pearson, O.N., DeCelles, P.G., 2005. Structural geology and regional tectonic significance of
1659 the Ramgarh thrust, Himalayan fold-thrust belt of Nepal. Tectonics 24, TC4008. doi:
1660 10.1029/2003TC001617
1661 Pennock, E.S., Lillie, R.J., Zaman, A.S.H., Yousuf, M., 1989. Structural Interpretation of Seismic
1662 Reflection Data from Eastern Salt Range and Potwar Plateau, Pakistan. AAPG Bull.
1663 73(7), 841-857. doi: 10.1306/44B4A27B-170A-11D7-8645000102C1865D
1664 Pierce, I., Wesnousky, S.G., 2016. On a flawed conclusion that the 1255 A.D. earthquake
1665 ruptured 800 km of the Himalayan Frontal Thrust east of Kathmandu. Geophys. Res.
1666 Lett. 43, 9026–9029. doi: 10.1002/2016GL070426
1667 Priyanka, R.S., Jayangondaperumal, R., Pandey, A., Mishra, R.L., Singh, I., Bhushan, R.,
1668 Srivastava, P., Ramachandran, S., Shah, C., Kedia, S., Sharma, A.K., Bhat, G.R., 2017.

1669 Primary surface rupture of the 1950 Tibet-Assam great earthquake along the eastern
1670 Himalayan front, India. Sci. Rep. 7, 5433. doi: 10.1038/s41598-017-05644-y

1671 Powers, P.M., Lillie, R.J., Yeats, R.S., 1998. Structure and shortening of the Kangra and Dehra
1672 Dun reentrants, Sub-Himalaya, India. Geol. Soc. Am. Bull. 110, 1010–1027.

1673 Raiverman, V., Chugh, M., Srivastava, A., Prasad, D., Das, S., 1994. Cenozoic tectonic of frontal
1674 fold belt of the Himalaya and Indo-Gangetic foredeep with pointers toward
1675 hydrocarbon prospects. Proceedings Second seminar on Petroliferous Basins of India,
1676 Dehra Dun, vol. 248001 pp. 25–54.

1677 Ramsey, B., 2009. Bayesian analysis of radiocarbon dates. Radiocarbon 51, 337-360.

1678 Reimer, P.J., Bard, E., Bayliss, A., Beck, J.W., Blackwell, P.G., Bronk Ramsey, C., Grootes, P.M.,
1679 Guilderson, T. P., Haflidason, H., Hajdas, I., HattŽ, C., Heaton, T.J., Hoffmann, D. L.,
1680 Hogg, A.G., Hughen, K.A., Kaiser, K.F., Kromer, B., Manning, S.W., Niu, M., Reimer,
1681 R.W., Richards, D.A., Scott, E.M., Southon, J.R., Staff, R.A., Turney, C. S.M., van der
1682 Plicht, J., 2013. IntCal13 and Marine13 Radiocarbon Age Calibration Curves 0-50,000
1683 Years cal BP. Radiocarbon, 55, 1869-1887. doi : 10.2458/azu_js_rc.55.16947

1684 Rizza, M., Bollinger, L., Sapkota, S. N., Tapponnier, P., Klinger, Y., Karakaş, Ç., Kali, E., Etchebes,
1685 M., Tiwari, D.R., Siwakoti, I., Bitri, A., Bes de Berc, S., 2019. Post earthquake
1686 aggradation processes to hide surface ruptures in thrust systems: The M8.3, 1934,
1687 Bihar-Nepal earthquake ruptures at Charnath Khola (Eastern Nepal). J. Geophys. Res.:
1688 Solid Earth, 124, 9182–9207. doi: 10.1029/2018JB016376

1689 Robert, X., 2009. Séquence d'activité des failles et dynamique du prisme himalayen: apports
1690 de la thermochronologie et de la modélisation numérique. Doctoral Dissertation,
1691 Joseph Fourier, Grenoble 1. 336 p.

1692 Roy, D., Tandon, S., Singh, V., 2021. Drainage evolution in a Holocene landscape that hosted a
1693 'lost river' system in the Punjab-Haryana plains, NW India. Quat. Int. 585, 99-110. doi:
1694 10.1016/j.quaint.2021.01.029

1695 Sapkota, S.N., 2011. Surface rupture of 1934 Bihar-Nepal earthquake: implications for seismic
1696 hazard in Nepal Himalaya. Doctoral Dissertation, Institut de physique du globe, Paris.
1697 291 p. doi: 10068/885114

1698 Sapkota, S.N., Bollinger, L., Klinger, Y., Tapponnier, P., Gaudemer, Y., Tiwari, D., 2013. Primary
1699 surface ruptures of the great Himalayan earthquakes in 1934 and 1255. Nat. Geosci.
1700 6, 71–76. doi: 10.1038/ngeo1669

1701 Sastri, V. V., 1979. An overview of petroleum geotectonis of the region to the north and south
1702 of the Himalaya. Himalayan Geology seminar, section III, Oil and Natural Gas
1703 resources, Geol. Surv. India Misc. Publ., 41, 247–276, 1979.

1704 Schelling, D., Arita, K., 1991. Thrust tectonics, crustal shortening, and the structure of the far-
1705 eastern Nepal Himalaya. Tectonics 10, 851–862. doi: 10.1029/91TC01011

1706 Schelling, D., Cater, J., Seago, R., Ojha, T., 1991. A balanced cross-section across the Central
1707 Nepal Siwalik Hills; Hitauda to Amlekhganj. J. Fac. Sci., Hokkaido Univ., Series 4:
1708 Geology and Mineralogy 23, 1–9.

1709 Schumm, S.A., 1985. Patterns of alluvial rivers. Annu. Rev. Earth Planet. Sci. 13, 5–27. doi:
1710 10.1146/annurev.ea.13.050185.000253

1711 Schumm, S.A., Khan, H.R., 1972. Experimental Study of Channel Patterns. Geol. Soc. Am. Bull.
1712 83, 1755. doi: 10.1130/0016-7606(1972)83[1755:ESOCP]2.0.CO;2

1713 Seeber, L., Armbruster, J.G., 1981. Great Detachment Earthquakes Along the Himalayan Arc
1714 and Long-Term Forecasting. Simpson, D.W., Richards, P.G. (Eds.), AGU, Washington, D.
1715 C., pp. 259–277. doi: 10.1029/ME004p0259

1716 Singh, A.K., Jaiswal, M.K., Pattanaik, J.K., Dev, M., 2016. Luminescence chronology of alluvial
1717 fan in North Bengal, India: implications to tectonics and climate. Geochronometria
1718 43, 101-112. doi: 10.1515/geochr-2015-0037.
1719 Singh, V., Tandon, S.K., 2008. The Pinjaur dun (intermontane longitudinal valley) and
1720 associated active mountain fronts, NW Himalaya: tectonic geomorphology and
1721 morphotectonic evolution. Geomorphology 102(3–4):376–394
1722 Singh, I., Pandey, A., Mishra, R. L., Priyanka, R. S., Brice, A., Jayangondaperumal, R.,
1723 Srivastava,V., 2021. Evidence of the 1950 great Assam earthquake surface break along
1724 the Mishmi Thrust at Namche Barwa Himalayan Syntaxis. Geophys. Res. Lett., 48,
1725 e2020GL090893. doi: 10.1029/2020GL090893
1726 Singh, I.B., 1996. Geological evolution of Ganga Plain-an overview. J. Palaeontol. Soc. Ind. 41,
1727 99-137.
1728 Sinha, R., Friend, P.F., Switsur, V.R., 1996. Radiocarbon dating and sedimentation rates in the
1729 Holocene alluvial sediments of the northern Bihar plains, India. Geol. Mag. 133, 85–
1730 90. doi: 10.1017/S0016756800007263
1731 Sinha, R., Gibling, M.R., Jain, V., Tandon, S.K., 2005. Sedimentology and avulsion patterns of
1732 the anabranching Baghmati river in the Himalayan foreland basin, India. In: Blum, M.,
1733 Marriott, S. (Eds.), Fluvial Sedimentology. Spec. Paub. Int. Assoc. Sedimentol., 35, pp.
1734 181-196.
1735 Sinha, R., Kumar, R., Sinha, S., Tandon, S.K, Gibling, M.R. 2007. Late Cenozoic fluvial
1736 successions in northern and western India: an overview and synthesis. Quat. Sci. Rev.
1737 26, 2801–2822. doi: 10.1016/j.quascirev.2007.07.018
1738 Sinha, R., Tandon, S.K., Gibling, M.R., 2010. Shallow sub-surface stratigraphy of the Ganga
1739 basin, Himalayan foreland: present status and future perspectives. Quat. Int. 227, 81-
1740 86. doi: 10.1016/j.quaint.2010.07.015
1741 Srinivasan, S., Khar, B.M., 1996. Status of hydrocarbon exploration in northwest Himalaya and
1742 foredeep: contributions to stratigraphy and structure. Visesa Prakasana-Bharatiya
1743 Bhuvaijñanika Sarveksana 21, 295–405.
1744 Srivastava, P., Singh, I.B., Sharma, M., Singhvi, A.K., 2003. Luminescence chronometry and
1745 Late Quaternary geomorphic history of the Ganga Plain, India. Palaeogeogr.,
1746 Palaeoclimatol., Palaeoecol. 197, 15–41. doi: https://doi.org/10.1016/S0031-
1747 0182(03)00384-5
1748 Srivastava, V.,Mukul, M., 2020. Cataclastic strain from external thrust sheets in fold-thrust
1749 belts: Insights fromthe frontal IndianHimalaya. J.Asian Earth Sci. 188 (October 2019),
1750 104092. https://doi.org/10.1016/j.jseaes.2019.104092.
1751 Srivastava, V., Mukul, M., Mukul, M., 2017. Quaternary deformation in the Gorubathan
1752 recess: Insights on the structural and landscape evolution in the frontal Darjiling
1753 Himalaya. Quat. Int. 462, 138–161. doi: 10.1016/j.quaint.2017.05.004
1754 Starkel, L., Płoskonka, D., Adamiec, G., 2015. Reconstruction of Late Quaternary Neotectonic
1755 Movements and Fluvial Activity in Sikkimese-Bhutanese Himalayan Piedmont. Studia
1756 Geomorphologica Carpatho-Balcanica 49, 71-82. doi: 10.1515/sgcb-2015-0010
1757 Stöcklin, J., 1980. Geology of Nepal and its regional frame: Thirty-third William Smith Lecture.
1758 J. Geol. Soc. 137, 1–34. doi: 10.1144/gsjgs.137.1.0001
1759 Suppe, J., 1983. Geometry and kinematics of fault-bend folding. Am. J. Sci. 283, 684–721. doi:
1760 10.2475/ajs.283.7.684

1761 Suppe, J., 2014. Active folding of landscapes and sedimentary basins. In Proceedings 5th
1762 International INQUA Meeting on Paleoseismology, Active Tectonics and
1763 Archeoseismology (PATA) 21-27 September 2014, Busan, Korea. P. 23-26.
1764 Suppe, J., Medwedeff, D. A., 1990. Geometry and kinematics of fault-propagation folding.
1765 Eclogae Geologicae Helvetiae, 83, 409–454.
1766 Suppe, J., Connors, C. D., & Zhang, Y., 2004. Shear fault-bend folding. AAPG Memoir, 82, 303–
1767 323.
1768 Taral, S. 2017. Sedimentology of the Siwalik Group in the Tista Valley and Kameng River
1769 section, eastern Himalaya: depositional systems, paleogeography, and paleoclimate.
1770 PhD thesis, Calcutta University. 275 p.
1771 Taral, S., Chakraborty, T., 2018. Deltaic coastline of the Siwalik (Neogene) foreland basin:
1772 evidences from the Gish River section, Darjeeling Himalaya: Deltaic Sedimentation in
1773 the Siwalik Group. Geol. J. 53, 203–229. doi: 10.1002/gj.2886
1774 Thakur, V.C., Pandey, A.K., Suresh, N., 2007. Late Quaternary-Holocene evolution of Dun
1775 structure and the Himalayan Frontal fault zone of the Garhwal Sub-Himalaya, NW
1776 India. J. Asian Earth Sci. 29, 305–319. doi: 10.1016/j.jseaes.2006.02.002
1777 Thakur, V.C, M. Joshi, M., Jayangondaperumal, M., 2020. Active Tectonics of Himalayan
1778 Frontal Fault Zone in the Sub-Himalaya. In N. Gupta, S. K. Tandon (eds.), Geodynamics
1779 of the Indian Plate, Springer Geology, p. 439-466.
1780 Upreti, B., Nakata, T., Kumahara, Y., Yagi, H., Okumura, K., Rockwell, T., Virdi, N., Maemoku,
1781 H., 2000. The latest active faulting in southeast Nepal. Proceedings of the Hokudan
1782 International symposium and School in active faulting, Awaji Island Hyogo Japan, pp.
1783 533–536.
1784 Van der Beek, P., Robert, X., Mugnier, J.-L., Bernet, M., Huyghe, P., Labrin, E., 2006. Late
1785 Miocene – Recent exhumation of the central Himalaya and recycling in the foreland
1786 basin assessed by apatite fission-track thermochronology of Siwalik sediments, Nepal.
1787 Basin Res. 18, 413–434. doi: 10.1111/j.1365-2117.2006.00305.x
1788 Vassallo R., Mugnier, J.-L., Vignon V., Malik, M.A., Jayangondaperumal, R., Srivastava, P.,
1789 Jouanne, F., Carcaillet, J., 2015. Quaternary deformation and seismic hazard in
1790 Northwestern Himalaya , Earth Planet. Sci. Lett., 411, 241–252. doi:
1791 10.1016/j.epsl.2014.11.030
1792 Vernant, P., Bilham, R., Szeliga, W., Drupka, D., Skalita, S., Bhattacharyya, A., Gaur, V.K.,
1793 Pelgay, P., Cattin, R., Berthet, T., 2014. Clockwise rotation of the Brahmaputra valley:
1794 tectonic convergence in the eastern Himalaya, Naga Hills and Shillong plateau. J.
1795 Geophys. Res. 119 (8), 6558e6571. http://dx.doi.org/10.1002/2014JB011196.
1796 Vignon, V., Mugnier, J.-L., Vassallo, R., Srivastava, P., Malik, M., Jayangondaperumal, R.,
1797 Jouanne, F., Buoncristiani, J.-F., Carcaillet, J., Replumaz, A., Jomard, H., 2017.
1798 Sedimentation close to the active Medlicott Wadia Thrust (Western Himalaya) : how
1799 to decipher tectonics and base level changes, Geomorphology 284, 175-190. doi:
1800 10.1016/j.geomorph.2016.07.040
1801 von Hagke, C., Malz, A., 2018. Triangle zones – Geometry, kinematics, mechanics, and the
1802 need for appreciation of uncertainties. Earth Science Reviews 177, 24-42
1803 Wahyudi, D.R., Sinclair, H. D., Mudd, S. M., 2021. Progressive evolution of thrust fold
1804 topography in the frontal Himalaya. Geomorphology 384, 107717. doi:
1805 10.1016/j.geomorph.2021.107717

1806 Wegmann, K.W., Pazzaglia, F.J., 2009. Late Quaternary fluvial terraces of the Romagna and
1807 Marche Apennines, Italy. Quat. Sci. Rev. 28, 137-165. doi:
1808 10.1016/j.quascirev.2008.10.006
1809 Weil, A.B., Yonkee, W.A., 2012. Layer-parallel shortening across the Sevier fold-thrust belt
1810 and Laramide foreland of Wyoming: spatial and temporal evolution of a complex
1811 geodynamic system. Earth Planet. Sci. Lett. 357–358, 405–420. doi:
1812 10.1016/j.epsl.2012.09.021
1813 Wesnousky, S.G., Kumahara, Y., Chamlagain, D., Neupane, P.C., 2019. Large Himalayan Frontal
1814 Thrust paleoearthquake at Khayarmara in eastern Nepal. J. Asian Earth Sci. 174, 346–
1815 351. doi: 10.1016/j.jseaes.2019.01.008
1816 Wesnousky, S.G., Kumahara, Y., Chamlagain, D., Pierce, I.K., Karki, A., Gautam, D., 2017a.
1817 Geological observations on large earthquakes along the Himalayan frontal fault near
1818 Kathmandu, Nepal. Earth Planet. Sci. Lett. 457, 366–375. doi:
1819 10.1016/j.epsl.2016.10.006
1820 Wesnousky, S.G., Kumahara, Y., Chamlagain, D., Pierce, I.K., Reedy, T., Angster, S.J., Giri, B.,
1821 2017b. Large paleoearthquake timing and displacement near Damak in eastern Nepal
1822 on the Himalayan Frontal Thrust. Geophys. Res. Lett. 44, 8219–8226. doi:
1823 10.1002/2017GL074270
1824 Wesnousky, S.G., Kumahara, Y., Nakata, T., Chamlagain, D., Neupane, P., 2018. New
1825 Observations Disagree With Previous Interpretations of Surface Rupture Along the
1826 Himalayan Frontal Thrust During the Great 1934 Bihar-Nepal Earthquake. Geophys.
1827 Res. Lett. 45, 2652–2658. doi: 10.1002/2018GL077035
1828 Whipple, K.X., Shirzaei, M., Hodges, K.V., Ramon Arrowsmith, J., 2016. Active shortening
1829 within the Himalayan orogenic wedge implied by the 2015 Gorkha earthquake. Nat.
1830 Geosci. 9, 711–716. doi: 10.1038/ngeo2797
1831 Wobus, C., Heimsath, A., Whipple, K., Hodges, K., 2005. Active out-of-sequence thrust
1832 faulting in the central Nepalese Himalaya. Nature 434, 1008–1011. doi:
1833 10.1038/nature03499
1834 Yeats, R.S., Thakur, V.C., 2008. Active faulting south of the Himalayan Front: Establishing a
1835 new plate boundary. Tectonophysics 453, 63–73. doi: 10.1016/j.tecto.2007.06.017
1836 Yhokha, A., Chang, C.-P., Goswami, P.K., Yen, J.-Y., Lee, S.-I., 2015. Surface deformation in the
1837 Himalaya and adjoining piedmont zone of the Ganga Plain, Uttarakhand, India:
1838 Determined by different radar interferometric techniques. J. Asian Earth Sci. 106,
1839 119–129. doi: 10.1016/j.jseaes.2015.02.032
1840 Yule, D., Dawson, S., Lavé, J., Sapkota, S., Tiwari, D., 2006. Possible Evidence for Surface
1841 Rupture of the Main Frontal Thrust During the Great 1505 Himalayan Earthquake, Far-
1842 Western Nepal. AGU Fall Meeting Abstracts, pp. S33C-05.
1843 Zhao, W., Nelson, K.D., Che, J., Quo, J., Lu, D., Wu, C., Liu, X., 1993. Deep seismic reflection
1844 evidence for continental underthrusting beneath southern Tibet. Nature 366, 557–
1845 559. doi: 10.1038/366557a0
1846